WAVE BACKSCATTERING BY POINT SCATTERERS IN THE RANDOM PARAXIAL REGIME

JOSSELIN GARNIER* AND KNUT SØLNA†

Abstract. When waves penetrate a medium without coherent reflectors, but with some fine scale medium heterogeneities, the backscattered wave is incoherent without any specific arrival time or the like. In this paper we consider a distributed field of microscatterers, like aerosols in the atmosphere, which coexists with microstructured clutter in the medium, like the fluctuations of the index of refraction of the turbulent atmosphere. We analyze the Wigner transform or the angularly resolved intensity profile of the backscattered wave when the incident wave is a beam in the paraxial regime. An enhanced backscattering phenomenon is proved and the properties of the enhanced backscattering cone (relative amplitude and profile) are shown to depend on the statistical parameters of the microstructure, but not on the microscatterers. These results are based on a multiscale analysis of the fourth-order moment of the fundamental solution of the white-noise paraxial wave equation. They pave the way for an estimation method of the statistical parameters of the microstructure from the observation of the enhanced backscattering cone. In our scaling argument we differentiate the two important canonical scaling regimes which are the scintillation regime and the spot dancing regime.

Key words. Waves in random media, parabolic approximation, scintillation, enhanced backscattering, turbulence estimation.

AMS subject classifications. 60H15, 35R60, 74J20.

1. Introduction. In this paper we consider the propagation of a beam in a turbulent medium in which imbedded particles play the role of point scatterers. These particles can be dust and aerosols in the turbulent atmosphere for instance. We consider the case in which the particles occupy an extended region and their density is invariant in the transverse direction (at least transversally invariant in the region illuminated by the incoming beam). The particles scatter light in all directions but we are only interested in the light that is backscattered and that can be collected in the same plane as the original source. The backscattering phenomena which are studied in this paper relate to single scattering from the particles imbedded in the turbulent medium and to complex interaction with the turbulent medium itself.

Our main goal is to study the dependence of the backscattered light with respect to the statistics of the random turbulent medium. The particle cloud plays the role of an uncontrolled source of backscattered light. We show that the mean backscattered intensity spatial profile does not depend on the statistical properties of the turbulent medium, but the covariance function of the backscattered waves, or equivalently the Wigner transform, depends on the statistical properties of the turbulent medium. In particular, by looking at the angular distribution of the backscattered energy flux, it is possible to exhibit an enhanced backscattering phenomenon and to relate the width of the enhanced backscattering cone and the enhancement factor to statistical parameters of the turbulent medium such as the Hurst exponent.

Enhanced backscattering or weak localization has been extensively discussed in the physical literature [3, 33] and observed in several experimental contexts [35, 32, 29, 22]. It usually refers to the situation that the mean backscattered power for a quasi-monochromatic quasi-plane has a local maximum in the backscattered direction,

[1]Laboratoire de Probabilités et Modèles Aléatoires & Laboratoire Jacques-Louis Lions, Université Paris Diderot, 75205 Paris Cedex 13, France garnier@math.univ-paris-diderot.fr

[2]Department of Mathematics, University of California, Irvine CA 92697 ksolna@math.uci.edu

which is twice as large as the mean backscattered power in the other directions. The classical enhanced backscattering phenomenon happens in a regime of multiple scattering by point scatterers and it results from the constructive interference of reciprocal light paths. In our paper we address a regime in which the waves experience single scattering by the point scatterers and the interaction of the waves with the turbulent medium is responsible for the enhanced backscattering phenomenon. Therefore, the properties of the cone depend on the statistical properties of the turbulent medium and not on the distribution of point scatterers.

In our paper the propagation through the turbulent medium is described by an Itô-Schrödinger equation [6]. This model is natural in many situations where a beam propagates mostly in the forward direction and the correlation length of the medium is much smaller than the propagation distance [4, 8, 9, 15, 25, 26, 27]. It allows for the use of Itô's stochastic calculus, which in turn enables the closure of the hierarchy of moment equations and the statistical analysis of important wave propagation problems, such as scintillation [2, 10, 12, 18, 30, 31, 34, 36] and in various applications to imaging and communication [1]. The analysis of the mean intensity and the Wigner transform of the backscattered wave involves fourth-order moments of the Green's function of the Itô-Schrödinger equation. The main theoretical result of this paper is a multiscale analysis of the fourth-order moments of the solution of the Itô-Schrödinger equation. This multiscale analysis allows to capture and characterize completely the narrow enhanced backscattering cone in the situation described above.

The paper is organized as follows. We briefly review the white-noise paraxial model in Section 2. We derive an integral representation of the covariance function of the backscattered field in Section 3, which shows that the fourth-order moments of the fundamental solutions are needed. We review the general moment equations in Section 4. We introduce two possible propagation regimes in Section 5 and we study the asymptotics of the covariance function of the backscattered field in these two regimes in Section 7. We give closed-form expressions for the Wigner distribution of the backscattered field in Section 8 and discuss the dependence of the enhanced backscattering cone with respect to the statistics of the random medium. Finally we carry out a few numerical simulations to illustrate the theoretical predictions in Section 9.

2. The White-Noise Paraxial Model. Let us consider the time-harmonic wave equation with homogeneous wavenumber k_0, random index of refraction $n(z,\boldsymbol{x})$, and source in the plane $z = z_{\rm i}$:

$$\Delta u + k_0^2 n^2(z,\boldsymbol{x}) u = -\delta(z - z_{\rm i}) f(\boldsymbol{x}). \tag{2.1}$$

Denote by λ_0 the carrier wavelength (equal to $2\pi/k_0$), by L the typical propagation distance, and by r_0 the radius of the initial transverse beam/source. The paraxial regime holds when the wavelength λ_0 is much smaller than the radius r_0, and when the propagation distance is at most of order r_0^2/λ_0 (the so-called Rayleigh length). The white-noise paraxial regime that we address in this paper holds when, additionally, the index of refraction of the medium has random fluctuations with a small typical amplitude and with correlation length much larger than the wavelength but smaller than the propagation distance. We refer to [16] for the explicit scaling assumptions. In this regime the solution of the time-harmonic wave equation (2.1) can be approximated by

$$u(z,\boldsymbol{x}) = \frac{i}{2k_0} \int f(\boldsymbol{x}_{\rm i}) G((z_{\rm i},\boldsymbol{x}_{\rm i}),(z,\boldsymbol{x})) d\boldsymbol{x}_{\rm i} \exp\big(ik_0|z - z_{\rm i}|\big),$$

where $(G((z_{\rm i},\boldsymbol{x}_{\rm i}),(z,\boldsymbol{x})))_{z\in\mathbb{R},\boldsymbol{x}\in\mathbb{R}^2}$ is the paraxial fundamental solution of the Itô-Schrödinger equation

$$dG(z,\boldsymbol{x})=\frac{i}{2k_0}\Delta_{\boldsymbol{x}}G(z,\boldsymbol{x})dz+\frac{ik_0}{2}G(z,\boldsymbol{x})\circ dB(z,\boldsymbol{x}), \tag{2.2}$$

with the initial condition in the plane $z=z_{\rm i}$:

$$G((z_{\rm i},\boldsymbol{x}_{\rm i}),(z=z_{\rm i},\boldsymbol{x}))=\delta(\boldsymbol{x}-\boldsymbol{x}_{\rm i}).$$

Here the symbol $\circ$ stands for the Stratonovich stochastic integral and $B(z,\boldsymbol{x})$ is a real-valued Brownian field over $\mathbb{R}\times\mathbb{R}^2$ with covariance

$$\mathbb{E}[B(z,\boldsymbol{x})B(z',\boldsymbol{x}')]=\min\{|z|,|z'|\}C(\boldsymbol{x}-\boldsymbol{x}'), \tag{2.3}$$

assuming $zz'>0$. The model (2.2) can be obtained from the scalar wave equation (2.1) by a separation of scales technique in which the three-dimensional fluctuations of the index of refraction $n(z,\boldsymbol{x})$ are described by a zero-mean stationary random process $\nu(z,\boldsymbol{x})$ with mixing properties: $n^2(z,\boldsymbol{x})=1+\nu(z,\boldsymbol{x})$. The covariance function $C(\boldsymbol{x})$ in (2.3) is then given in terms of the two-point statistics of the random process ν by

$$C(\boldsymbol{x})=\int_{-\infty}^{\infty}\mathbb{E}[\nu(z'+z,\boldsymbol{x}'+\boldsymbol{x})\nu(z',\boldsymbol{x}')]dz. \tag{2.4}$$

The covariance function C is assumed to decay fast enough at infinity so that it belongs to $L^1(\mathbb{R}^2)$. Its Fourier transform is nonnegative (since it is the power spectral density of the stationary process $\boldsymbol{x}\to B(1,\boldsymbol{x})$). The white-noise paraxial model is widely used in the physical literature [1]. It simplifies the full wave equation (2.1) by replacing it with an initial value-problem (2.2). It was studied mathematically in [6]. The proof of its derivation from the three-dimensional wave equation in randomly scattering medium uses tools presented in [11] and it is given in [16].

3. The Backscattered Field. We assume a Gaussian source in the plane $z=0$ with radius r_0 emitting toward $z<0$:

$$f(\boldsymbol{x})=\exp\big(-\frac{|\boldsymbol{x}|^2}{2r_0^2}\big).$$

We assume that there is a Poisson cloud (or Poisson point process [21]) giving point scatterers in the medium for $z<0$:

$$n_{\rm ps}^2(z,\boldsymbol{x})=\sum_j w_j\delta(\boldsymbol{x}-\boldsymbol{x}_j)\delta(z-z_j).$$

The time-harmonic field satisfies

$$\Delta u+k_0^2\big[n^2(z,\boldsymbol{x})+n_{\rm ps}^2(z,\boldsymbol{x})\big]u=-\delta(z)f(\boldsymbol{x}).$$

Using the Born (or single-scattering) approximation for the point scatterers, the backscattered field recorded in the plane $z=0$ at $(0,\boldsymbol{x}_r)$ is

$$u(0,\boldsymbol{x}_r)=-\frac{1}{4}\sum_j\exp\big(2ik_0|z_j|\big)\int d\boldsymbol{x}_0 f(\boldsymbol{x}_0)G((0,\boldsymbol{x}_0),(z_j,\boldsymbol{x}_j))w_jG((z_j,\boldsymbol{x}_j),(0,\boldsymbol{x}_r)). \tag{3.1}$$

The use of the paraxial fundamental solution G is justified because the point scatterers playing the roles of secondary sources are along the z-axis (in a tube that is illuminated by the incident beam) and the field is collected in the plane $z = 0$ but close to the z-axis as well.

In this paper we assume that the intensity $\rho_{\rm ps}(z)$ of the Poisson cloud depends only on z. In practice our results can be extended to the case when the intensity of the Poisson cloud varies laterally on a scale that is slow relative to the beam width. It is assumed to be supported in the region $z < 0$ away from 0. The scale of variation of the function $\rho_{\rm ps}(z)$ is assumed to be much larger than the wavelength. The reflectivities w_j of the scatterers can be deterministic or random, we denote by σ^2 their second moment and by $\bar{w}$ their first moment. In this configuration the mean of the backscattered field is:

$$\begin{aligned}\Big\langle u(0,\boldsymbol{x}_r)\Big\rangle = -\frac{\bar{w}}{4}\int_{-\infty}^{0} dz_{\rm i}\rho_{\rm ps}(z_{\rm i})\exp\big(-2ik_0z_{\rm i}\big)\int d\boldsymbol{x}_{\rm i}\int d\boldsymbol{x}_0 f(\boldsymbol{x}_0)\\ \times G((0,\boldsymbol{x}_0),(z_{\rm i},\boldsymbol{x}_{\rm i}))G((z_{\rm i},\boldsymbol{x}_{\rm i}),(0,\boldsymbol{x}_r)),\end{aligned} \tag{3.2}$$

where $\langle\cdot\rangle$ stands for the expectation with respect to the distribution of the point scatterers. This equation follows from the general result that, for a Poisson point process with intensity $\rho(z,\boldsymbol{x})$, we have for any test function $g(z,\boldsymbol{x})$ [21, Eq. (3.9)]:

$$\Big\langle \sum_j g(z_j,\boldsymbol{x}_j)\Big\rangle = \int g(z,\boldsymbol{x})\rho(z,\boldsymbol{x})dzd\boldsymbol{x}.$$

The presence of the rapid phase $\exp(-2ik_0z_{\rm i})$ in (3.2) averages out the integral to zero, which shows that the backscattered field has mean zero:

$$\Big\langle u(0,\boldsymbol{x}_r)\Big\rangle = 0. \tag{3.3}$$

This result means that the backscattered wave is incoherent. The covariance function of the backscattered field is our main quantity of interest:

$$\begin{aligned}\Big\langle u(0,\boldsymbol{x}_r)\overline{u(0,\boldsymbol{x}_r')}\Big\rangle = \frac{\sigma^2}{16}\int_{-\infty}^{0} dz_{\rm i}\rho_{\rm ps}(z_{\rm i})\int d\boldsymbol{x}_{\rm i}\iint d\boldsymbol{x}_0 d\boldsymbol{x}_0' f(\boldsymbol{x}_0)f(\boldsymbol{x}_0')\\ \times G((0,\boldsymbol{x}_0),(z_{\rm i},\boldsymbol{x}_{\rm i}))G((z_{\rm i},\boldsymbol{x}_{\rm i}),(0,\boldsymbol{x}_r))\overline{G((0,\boldsymbol{x}_0'),(z_{\rm i},\boldsymbol{x}_{\rm i}))G((z_{\rm i},\boldsymbol{x}_{\rm i}),(0,\boldsymbol{x}_r'))}.\end{aligned}$$

This equation follows from the general result that, for a Poisson point process with intensity $\rho(z,\boldsymbol{x})$, we have for any test function $g(z,\boldsymbol{x})$ [21, Eq. (3.10)]:

$$\Big\langle \Big|\sum_j g(z_j,\boldsymbol{x}_j)\Big|^2\Big\rangle = \int |g(z,\boldsymbol{x})|^2\rho(z,\boldsymbol{x})dzd\boldsymbol{x} + \Big|\int g(z,\boldsymbol{x})\rho(z,\boldsymbol{x})dzd\boldsymbol{x}\Big|^2.$$

Using reciprocity we have

$$G((0,\boldsymbol{x}_0),(z_{\rm i},\boldsymbol{x}_{\rm i})) = G((z_{\rm i},\boldsymbol{x}_{\rm i}),(0,\boldsymbol{x}_0)) \text{ and } G((0,\boldsymbol{x}_0'),(z_{\rm i},\boldsymbol{x}_{\rm i})) = G((z_{\rm i},\boldsymbol{x}_{\rm i}),(0,\boldsymbol{x}_0')).$$

Therefore,

$$\begin{aligned}\Big\langle u(0,\boldsymbol{x}_r)\overline{u(0,\boldsymbol{x}_r')}\Big\rangle = \frac{\sigma^2}{16}\int_{-\infty}^{0} dz_{\rm i}\rho_{\rm ps}(z_{\rm i})\int d\boldsymbol{x}_{\rm i}\iint d\boldsymbol{x}_0 d\boldsymbol{x}_0' f(\boldsymbol{x}_0)f(\boldsymbol{x}_0')\\ \times G((z_{\rm i},\boldsymbol{x}_{\rm i}),(0,\boldsymbol{x}_0))G((z_{\rm i},\boldsymbol{x}_{\rm i}),(0,\boldsymbol{x}_r))\overline{G((z_{\rm i},\boldsymbol{x}_{\rm i}),(0,\boldsymbol{x}_0'))G((z_{\rm i},\boldsymbol{x}_{\rm i}),(0,\boldsymbol{x}_r'))}.\end{aligned}$$

Using the statistical homogeneity of the random medium we have in distribution (with respect to the distribution of the random medium) for any $z_\mathrm{i} < 0$:

$$(G((z_\mathrm{i}, \boldsymbol{x}_\mathrm{i}), (0, \boldsymbol{x})))_{\boldsymbol{x}\in\mathbb{R}^2} \overset{\text{dist.}}{=} (G((0, \boldsymbol{x}_\mathrm{i}), (|z_\mathrm{i}|, \boldsymbol{x})))_{\boldsymbol{x}\in\mathbb{R}^2}.$$

Therefore, by taking the expectation with respect to the distribution of the point scatterers and the distribution of the random medium, we have

$$\mathbb{E}[u(0, \boldsymbol{x}_r)\overline{u(0, \boldsymbol{x}'_r)}] = \frac{\sigma^2}{16}\int_0^\infty dz\rho(z)\int d\boldsymbol{x}_\mathrm{i}\iint d\boldsymbol{x}_0 d\boldsymbol{x}'_0 f(\boldsymbol{x}_0)f(\boldsymbol{x}'_0)$$
$$\times\mathbb{E}\Big[G((0, \boldsymbol{x}_\mathrm{i}), (z, \boldsymbol{x}_0))G((0, \boldsymbol{x}_\mathrm{i}), (z, \boldsymbol{x}_r))\overline{G((0, \boldsymbol{x}_\mathrm{i}), (z, \boldsymbol{x}'_0))G((0, \boldsymbol{x}_\mathrm{i}), (z, \boldsymbol{x}'_r))}\Big], \quad (3.4)$$

where $\rho(z) = \rho_\mathrm{ps}(-z)$. This equation shows that we need to compute the fourth-order moment of the paraxial fundamental solution. In fact we only need to compute the integral over $\boldsymbol{x}_\mathrm{i}$ of this quantity, which is in fact simpler.

If the source is not time-harmonic, but a pulse with carrier frequency ω_0 that is emitted at time 0, and if the recorded wave is time-windowed within the time-interval $[T_1, T_2]$, then the time integrated covariance function of the backscattered wave

$$\frac{1}{(2\pi)^2}\int_{T_1}^{T_2}\mathbb{E}[u(t, 0, \boldsymbol{x}_r)u(t, 0, \boldsymbol{x}'_r)]dt$$

is given by an integral of type (3.4) where $k_0 = \omega_0/c_0$ is the carrier wavenumber (with c_0 the background wave speed) and the integral in z is essentially limited to $[z_1, z_2]$ with $z_j = c_0 T_j/2$. Note that, if the pulse is broadband in the sense that the bandwidth is of the same order as the carrier frequency, then we need to integrate (3.4) over the bandwidth. We will only consider narrowband pulses in our paper. This time-windowing technique is a practical way to select the propagation distance that is probed by the reflection method.

4. The General Moment Equations. The main tool for describing wave statistics are the finite-order moments. We show in this section that in the context of the Itô-Schrödinger equation (2.2) the moments of the field satisfy a closed system at each order [20, 12]. For $\boldsymbol{x}_\mathrm{i} \in \mathbb{R}^2$, $p \in \mathbb{N}$, we define

$$M^{(p)}_{\boldsymbol{x}_\mathrm{i}}\big(z, (\boldsymbol{x}_j)_{j=1}^p, (\boldsymbol{y}_l)_{l=1}^p\big) = \mathbb{E}\Big[\prod_{j=1}^p G((0, \boldsymbol{x}_\mathrm{i}), (z, \boldsymbol{x}_j))\prod_{l=1}^p\overline{G((0, \boldsymbol{x}_\mathrm{i}), (z, \boldsymbol{y}_l))}\Big], \quad (4.1)$$

for $(\boldsymbol{x}_j)_{j=1}^p, (\boldsymbol{y}_l)_{l=1}^p \in \mathbb{R}^{2p}$. Using the stochastic equation (2.2) and Itô's formula for Hilbert space valued processes [24], we find that the function $M^{(p)}_{\boldsymbol{x}_\mathrm{i}}$ satisfies the Schrödinger-type system:

$$\frac{\partial M^{(p)}_{\boldsymbol{x}_\mathrm{i}}}{\partial z} = \frac{i}{2k_0}\Big(\sum_{j=1}^p\Delta_{\boldsymbol{x}_j} - \sum_{l=1}^p\Delta_{\boldsymbol{y}_l}\Big)M^{(p)}_{\boldsymbol{x}_\mathrm{i}} + \frac{k_0^2}{4}U_p\big((\boldsymbol{x}_j)_{j=1}^p, (\boldsymbol{y}_l)_{l=1}^p\big)M^{(p)}_{\boldsymbol{x}_\mathrm{i}}, \quad (4.2)$$

$$M^{(p)}_{\boldsymbol{x}_\mathrm{i}}(z=0) = \prod_{j=1}^p\delta(\boldsymbol{x}_j - \boldsymbol{x}_\mathrm{i})\prod_{l=1}^p\delta(\boldsymbol{y}_l - \boldsymbol{x}_\mathrm{i}), \quad (4.3)$$

with the generalized potential

$$U_p\big((\boldsymbol{x}_j)_{j=1}^p,(\boldsymbol{y}_l)_{l=1}^p\big)=\sum_{j,l=1}^p C(\boldsymbol{x}_j-\boldsymbol{y}_l)-\frac{1}{2}\sum_{j,j'=1}^p C(\boldsymbol{x}_j-\boldsymbol{x}_{j'})-\frac{1}{2}\sum_{l,l'=1}^p C(\boldsymbol{y}_l-\boldsymbol{y}_{l'})$$

$$=\sum_{j,l=1}^p C(\boldsymbol{x}_j-\boldsymbol{y}_l)-\sum_{1\le j<j'\le p} C(\boldsymbol{x}_j-\boldsymbol{x}_{j'})-\sum_{1\le l<l'\le p} C(\boldsymbol{y}_l-\boldsymbol{y}_{l'})-pC(\boldsymbol{0}). \tag{4.4}$$

We introduce the Fourier transform

$$\hat{M}^{(p)}_{\boldsymbol{x}_{\rm i}}\big(z,(\boldsymbol{\xi}_j)_{j=1}^p,(\boldsymbol{\zeta}_l)_{l=1}^p\big)=\iint M^{(p)}_{\boldsymbol{x}_{\rm i}}\big(z,(\boldsymbol{x}_j)_{j=1}^p,(\boldsymbol{y}_l)_{l=1}^p\big)$$
$$\times\exp\Big(-i\sum_{j=1}^p\boldsymbol{x}_j\cdot\boldsymbol{\xi}_j+i\sum_{l=1}^p\boldsymbol{y}_l\cdot\boldsymbol{\zeta}_l\Big)d\boldsymbol{x}_1\cdots d\boldsymbol{x}_p d\boldsymbol{y}_1\cdots d\boldsymbol{y}_p. \tag{4.5}$$

It satisfies

$$\frac{\partial\hat{M}^{(p)}_{\boldsymbol{x}_{\rm i}}}{\partial z}=-\frac{i}{2k_0}\Big(\sum_{j=1}^p|\boldsymbol{\xi}_j|^2-\sum_{l=1}^p|\boldsymbol{\zeta}_l|^2\Big)\hat{M}^{(p)}_{\boldsymbol{x}_{\rm i}}+\frac{k_0^2}{4}\hat{\mathcal{U}}_p\hat{M}^{(p)}_{\boldsymbol{x}_{\rm i}}, \tag{4.6}$$

$$\hat{M}^{(p)}_{\boldsymbol{x}_{\rm i}}(z=0)=\exp\Big(-i\sum_{j=1}^p\boldsymbol{x}_{\rm i}\cdot\boldsymbol{\xi}_j+i\sum_{l=1}^p\boldsymbol{x}_{\rm i}\cdot\boldsymbol{\zeta}_l\Big). \tag{4.7}$$

In Eq. (4.6) the operator $\hat{\mathcal{U}}_p$ is defined by

$$\hat{\mathcal{U}}_p\hat{M}^{(p)}_{\boldsymbol{x}_{\rm i}}=\frac{1}{(2\pi)^2}\int\hat{C}(\boldsymbol{k})\Big[\sum_{j,l=1}^p\hat{M}^{(p)}_{\boldsymbol{x}_{\rm i}}(\boldsymbol{\xi}_j-\boldsymbol{k},\boldsymbol{\zeta}_l-\boldsymbol{k})-\sum_{1\le j<j'\le p}\hat{M}^{(p)}_{\boldsymbol{x}_{\rm i}}(\boldsymbol{\xi}_j-\boldsymbol{k},\boldsymbol{\xi}_{j'}+\boldsymbol{k})$$
$$-\sum_{1\le l<l'\le p}\hat{M}^{(p)}_{\boldsymbol{x}_{\rm i}}(\boldsymbol{\zeta}_l-\boldsymbol{k},\boldsymbol{\zeta}_{l'}+\boldsymbol{k})-p\hat{M}^{(p)}_{\boldsymbol{x}_{\rm i}}\Big]d\boldsymbol{k}, \tag{4.8}$$

where we only write the arguments that are shifted. It turns out that the equation (4.6) for the Fourier transform $\hat{M}^{(p)}_{\boldsymbol{x}_{\rm i}}$ is easier to solve than (4.2). In particular it can be integrated readily if the medium is homogeneous.

5. Regimes of Propagation. In order to get closed-form expressions for some relevant quantities, we will address the two following particular regimes, which can be considered as particular cases of the paraxial white-noise regime. Let us denote by ϑ the standard deviation of the fluctuations of the index of refraction and by l_z (resp. l_x) the longitudinal (resp. transverse) correlation length of the fluctuations of the index of refraction. Then the correlation length in the propagation direction, $C(\boldsymbol{0})$, is of order $\vartheta^2 l_z$ and the transverse scale of variation of $C(\boldsymbol{x})$ is of order l_x. As before, λ_0 is the carrier wavelength (equal to $2\pi/k_0$), L is the typical propagation distance, and r_0 is the radius of the initial transverse beam/source. In this notation the Rayleigh length, which corresponds to the distance when the transverse radius of the beam roughly has doubled by diffraction in the homogeneous medium case, is r_0^2/λ_0. Moreover, as seen in (4.2) $k_0^2C(\boldsymbol{0})L$ or $\vartheta^2 l_z L/\lambda_0^2$ is a measure of the relative strength of the medium fluctuations over the propagation distance. In what follows, ε is a small dimensionless parameter.

- *The spot-dancing regime.* The random medium fluctuations are relatively strong, so that $\vartheta^2 l_z L/\lambda_0^2$ is of order $1/\varepsilon^2$, the initial beam support is small, so that r_0/l_x is of order ε, and the propagation distance is such that $L\lambda_0/r_0^2$ is of order one (ie the typical propagation distance is of the order of the Rayleigh length of the initial beam). This leads to a picture where the transmitted wave field center "dances" according to a random frame [6, 18].
- *The scintillation regime.* The random medium fluctuations are relatively weak, so that $\vartheta^2 l_z L/\lambda_0^2$ is of order one, the initial beam support is broad, so that r_0/l_x is of order $1/\varepsilon$, while the propagation distance is such that $L\lambda_0/r_0^2$ is of order $1/\varepsilon$ (ie the typical propagation distance is relatively large compared to the Rayleigh length of the initial beam). This leads to a picture consistent with random and Gaussian fluctuations for the transmitted field [18].

5.1. The Spot-Dancing Regime. In this subsection we review the results that can be found in [1, 6, 13, 14] and put them in a convenient form for the forthcoming analysis. In this regime the covariance function C^ε is of the form:

$$C^\varepsilon(\boldsymbol{x}) = \varepsilon^{-2} C(\varepsilon \boldsymbol{x}), \tag{5.1}$$

for a small dimensionless parameter ε. We want to study the asymptotic behavior of the moments of the field in this regime, that we call spot-dancing regime for reasons that will become clear in the analysis.

In the spot-dancing regime we assume that the power spectral density $\hat{C}(\boldsymbol{k})$ decays fast enough so that $\int |\boldsymbol{k}|^4 \hat{C}(\boldsymbol{k}) d\boldsymbol{k}$ is finite. This implies that the covariance function $C(\boldsymbol{x})$ is at least four times differentiable at $\boldsymbol{x} = \boldsymbol{0}$, which corresponds to a smooth random medium. For simplicity, we also assume that the random fluctuations are isotropic in the transverse directions, in the sense that the covariance function $C(\boldsymbol{x})$ depends only on $|\boldsymbol{x}|$. We denote

$$\gamma = \frac{1}{2(2\pi)^2} \int |\boldsymbol{k}|^2 \hat{C}(\boldsymbol{k}) d\boldsymbol{k} = -\frac{1}{2} \Delta C(\boldsymbol{0}). \tag{5.2}$$

The operator $\hat{\mathcal{U}}_p^\varepsilon$ has then the form

$$\begin{aligned} \hat{\mathcal{U}}_p^\varepsilon \hat{M}_{\boldsymbol{x}_{\rm i}}^{(p)} = \frac{\varepsilon^{-2}}{(2\pi)^2} \int \hat{C}(\boldsymbol{k}) \Big[\sum_{j,l=1}^{p} \hat{M}_{\boldsymbol{x}_{\rm i}}^{(p)}(\boldsymbol{\xi}_j - \varepsilon \boldsymbol{k}, \boldsymbol{\zeta}_l - \varepsilon \boldsymbol{k}) \\ - \sum_{1 \le j < j' \le p} \hat{M}_{\boldsymbol{x}_{\rm i}}^{(p)}(\boldsymbol{\xi}_j - \varepsilon \boldsymbol{k}, \boldsymbol{\xi}_{j'} + \varepsilon \boldsymbol{k}) \\ - \sum_{1 \le l < l' \le p} \hat{M}_{\boldsymbol{x}_{\rm i}}^{(p)}(\boldsymbol{\zeta}_l - \varepsilon \boldsymbol{k}, \boldsymbol{\zeta}_{l'} + \varepsilon \boldsymbol{k}) - p \hat{M}_{\boldsymbol{x}_{\rm i}}^{(p)} \Big] d\boldsymbol{k}, \end{aligned} \tag{5.3}$$

and it can be expanded as $\varepsilon \to 0$ as

$$\hat{\mathcal{U}}_p^\varepsilon \hat{M}_{\boldsymbol{x}_{\rm i}}^{(p)} = \frac{\gamma}{2} \Big(\sum_{j=1}^{p} \nabla_{\boldsymbol{\xi}_j} + \sum_{l=1}^{p} \nabla_{\boldsymbol{\zeta}_l} \Big) \cdot \Big(\sum_{j=1}^{p} \nabla_{\boldsymbol{\xi}_j} + \sum_{l=1}^{p} \nabla_{\boldsymbol{\zeta}_l} \Big) \hat{M}_{\boldsymbol{x}_{\rm i}}^{(p)}.$$

As shown in [6, 18], this implies that, in the regime $\varepsilon \to 0$, the function $\hat{M}_{\boldsymbol{x}_{\rm i}}^{(p)}$ satisfies

the partial differential equation

$$\frac{\partial \hat{M}^{(p)}_{\boldsymbol{x}_{\rm i}}}{\partial z} = -\frac{i}{2k_0}\Big(\sum_{j=1}^{p}|\boldsymbol{\xi}_j|^2 - \sum_{l=1}^{p}|\boldsymbol{\zeta}_l|^2\Big)\hat{M}^{(p)}_{\boldsymbol{x}_{\rm i}} + \frac{k_0^2\gamma}{8}\Big(\sum_{j=1}^{p}\nabla_{\boldsymbol{\xi}_j} + \sum_{l=1}^{p}\nabla_{\boldsymbol{\zeta}_l}\Big)\cdot\Big(\sum_{j=1}^{p}\nabla_{\boldsymbol{\xi}_j} + \sum_{l=1}^{p}\nabla_{\boldsymbol{\zeta}_l}\Big)\hat{M}^{(p)}_{\boldsymbol{x}_{\rm i}}. \tag{5.4}$$

Using the Feynman-Kac formula, we find that

$$\hat{M}^{(p)}_{\boldsymbol{x}_{\rm i}}\big(z,(\boldsymbol{\xi}_j)_{j=1}^p,(\boldsymbol{\zeta}_l)_{l=1}^p\big) = \mathbb{E}\Big[\prod_{j=1}^{p}G_{{\rm sd},\boldsymbol{x}_{\rm i}}(z,\boldsymbol{\xi}_j)\prod_{l=1}^{p}\overline{G_{{\rm sd},\boldsymbol{x}_{\rm i}}(z,\boldsymbol{\zeta}_l)}\Big], \tag{5.5}$$

where

$$G_{{\rm sd},\boldsymbol{x}_{\rm i}}(z,\boldsymbol{\xi}) = \exp\Big(-i\boldsymbol{x}_{\rm i}\cdot\big(\boldsymbol{\xi}+\frac{k_0\sqrt{\gamma}}{2}\boldsymbol{W}_z\big) - \frac{i}{2k_0}\int_0^z\big|\boldsymbol{\xi}+\frac{k_0\sqrt{\gamma}}{2}\boldsymbol{W}_{z'}\big|^2dz'\Big), \tag{5.6}$$

and $\boldsymbol{W}_z$ is a standard 2-dimensional Brownian motion. Of course, when $\gamma = 0$, we recover the expression of the field in the homogeneous case. A detailed statistical analysis of the field can then be carried out [18], which shows that the shape of the spatial profile of the transmitted wave field evolves as in a homogeneous medium, but its center is randomly shifted and follows Gaussian statistics that can be fully characterized. The random shift of the center is the origin of the term "spot dancing".

5.2. The Scintillation Regime. In this subsection we consider the scintillation regime described at the end of Section 2. In this regime the covariance function C^ε is of the form:

$$C^\varepsilon(\boldsymbol{x}) = \varepsilon C(\boldsymbol{x}). \tag{5.7}$$

and the radius of the initial source is of order $1/\varepsilon$, we will denote it by r_0/ε. In order to observe a random effect of order one, we need to consider propagation distances of the order of ε^{-1}. Therefore we assume that the density $\rho(z)$ has the form $\varepsilon\rho(\varepsilon z)$ and we make the rescaling $z = z'/\varepsilon$ and suppress the "prime" below. This regime is called the scintillation regime by the results obtained in [18] that show that the fluctuations of the transmitted field have some statistical characteristics similar to those of complex Gaussian processes. The evolution equations (4.6) of the Fourier transforms of the moments now become

$$\frac{\partial \hat{M}^{(p)}_{\boldsymbol{x}_{\rm i}}}{\partial z} = -\frac{i}{2k_0\varepsilon}\Big(\sum_{j=1}^{p}|\boldsymbol{\xi}_j|^2 - \sum_{l=1}^{p}|\boldsymbol{\zeta}_l|^2\Big)\hat{M}^{(p)}_{\boldsymbol{x}_{\rm i}} + \frac{k_0^2}{4}\hat{\mathcal{U}}_p\hat{M}^{(p)}_{\boldsymbol{x}_{\rm i}}, \tag{5.8}$$

which shows the appearance of a rapid phase. The asymptotic behavior as $\varepsilon \to 0$ of the moments is therefore determined by the solutions of partial differential equations with rapid phase terms. Although we will not determine the asymptotic behaviors for all moments, a key limit theorem will allow us to get a representation of the fourth-order moments in the limit $\varepsilon \to 0$.

6. The Fourth-Order Moments. We consider the fourth-order moment $M^{(2)}_{\boldsymbol{x}_{\rm i}}$ of the field, which is the main quantity of interest in this paper. In this section we consider the fourth-order moments in the general case and in subsequent sections we

will then specialize two the regimes corresponding to spot dancing and scintillation. First we parameterize the four points $\boldsymbol{x}_1, \boldsymbol{x}_2, \boldsymbol{y}_1, \boldsymbol{y}_2$ in (4.1) as:

$$\begin{aligned} \boldsymbol{x}_1 &= \frac{\boldsymbol{r}_1 + \boldsymbol{r}_2 + \boldsymbol{q}_1 + \boldsymbol{q}_2}{2}, \qquad \boldsymbol{y}_1 = \frac{\boldsymbol{r}_1 + \boldsymbol{r}_2 - \boldsymbol{q}_1 - \boldsymbol{q}_2}{2}, \\ \boldsymbol{x}_2 &= \frac{\boldsymbol{r}_1 - \boldsymbol{r}_2 + \boldsymbol{q}_1 - \boldsymbol{q}_2}{2}, \qquad \boldsymbol{y}_2 = \frac{\boldsymbol{r}_1 - \boldsymbol{r}_2 - \boldsymbol{q}_1 + \boldsymbol{q}_2}{2}. \end{aligned}$$

In particular $\boldsymbol{r}_1/2$ is the barycenter of the four points $\boldsymbol{x}_1, \boldsymbol{x}_2, \boldsymbol{y}_1, \boldsymbol{y}_2$:

$$\begin{aligned} \boldsymbol{r}_1 &= \frac{\boldsymbol{x}_1 + \boldsymbol{x}_2 + \boldsymbol{y}_1 + \boldsymbol{y}_2}{2}, \qquad \boldsymbol{q}_1 = \frac{\boldsymbol{x}_1 + \boldsymbol{x}_2 - \boldsymbol{y}_1 - \boldsymbol{y}_2}{2}, \\ \boldsymbol{r}_2 &= \frac{\boldsymbol{x}_1 - \boldsymbol{x}_2 + \boldsymbol{y}_1 - \boldsymbol{y}_2}{2}, \qquad \boldsymbol{q}_2 = \frac{\boldsymbol{x}_1 - \boldsymbol{x}_2 - \boldsymbol{y}_1 + \boldsymbol{y}_2}{2}. \end{aligned}$$

In these new variables the function $M^{(2)}_{\boldsymbol{x}_\mathrm{i}}$ satisfies the system:

$$\frac{\partial M^{(2)}_{\boldsymbol{x}_\mathrm{i}}}{\partial z} = \frac{i}{k_0}\big(\nabla_{\boldsymbol{r}_1} \cdot \nabla_{\boldsymbol{q}_1} + \nabla_{\boldsymbol{r}_2} \cdot \nabla_{\boldsymbol{q}_2}\big) M^{(2)}_{\boldsymbol{x}_\mathrm{i}} + \frac{k_0^2}{4} U_2(\boldsymbol{q}_1, \boldsymbol{q}_2, \boldsymbol{r}_1, \boldsymbol{r}_2) M^{(2)}_{\boldsymbol{x}_\mathrm{i}}, \tag{6.1}$$

starting from $M^{(2)}_{\boldsymbol{x}_\mathrm{i}}(z = 0, \boldsymbol{q}_1, \boldsymbol{q}_2, \boldsymbol{r}_1, \boldsymbol{r}_2) = \delta(\boldsymbol{q}_1)\delta(\boldsymbol{q}_2)\delta(\boldsymbol{r}_1 - 2\boldsymbol{x}_\mathrm{i})\delta(\boldsymbol{r}_2)$, with the generalized potential

$$\begin{aligned} U_2(\boldsymbol{q}_1, \boldsymbol{q}_2, \boldsymbol{r}_1, \boldsymbol{r}_2) = {} & C(\boldsymbol{q}_2 + \boldsymbol{q}_1) + C(\boldsymbol{q}_2 - \boldsymbol{q}_1) + C(\boldsymbol{r}_2 + \boldsymbol{q}_1) + C(\boldsymbol{r}_2 - \boldsymbol{q}_1) \\ & - C(\boldsymbol{q}_2 + \boldsymbol{r}_2) - C(\boldsymbol{q}_2 - \boldsymbol{r}_2) - 2C(\boldsymbol{0}). \end{aligned} \tag{6.2}$$

Note in particular that the generalized potential does not depend on $\boldsymbol{r}_1$ as the medium is statistically homogeneous.

The Fourier transform (in $\boldsymbol{q}_1$, $\boldsymbol{q}_2$, $\boldsymbol{r}_1$, and $\boldsymbol{r}_2$) of the fourth-order moment is defined by:

$$\begin{aligned} \hat{M}^{(2)}_{\boldsymbol{x}_\mathrm{i}}(z, \boldsymbol{\xi}_1, \boldsymbol{\xi}_2, \boldsymbol{\zeta}_1, \boldsymbol{\zeta}_2) = {} & \iint M^{(2)}_{\boldsymbol{x}_\mathrm{i}}(z, \boldsymbol{q}_1, \boldsymbol{q}_2, \boldsymbol{r}_1, \boldsymbol{r}_2) \\ & \times \exp\big(-i\boldsymbol{q}_1 \cdot \boldsymbol{\xi}_1 - i\boldsymbol{r}_1 \cdot \boldsymbol{\zeta}_1 - i\boldsymbol{q}_2 \cdot \boldsymbol{\xi}_2 - i\boldsymbol{r}_2 \cdot \boldsymbol{\zeta}_2\big) d\boldsymbol{r}_1 d\boldsymbol{r}_2 d\boldsymbol{q}_1 d\boldsymbol{q}_2. \end{aligned} \tag{6.3}$$

PROPOSITION 6.1. *The Fourier transform $\hat{M}^{(2)}_{\boldsymbol{x}_\mathrm{i}}$ of the fourth-order moment satisfies*

$$\int d\boldsymbol{x}_\mathrm{i} \hat{M}^{(2)}_{\boldsymbol{x}_\mathrm{i}}(z, \boldsymbol{\xi}_1, \boldsymbol{\xi}_2, \boldsymbol{\zeta}_1, \boldsymbol{\zeta}_2) = \pi^2 \hat{M}(z, \boldsymbol{\xi}_2, \boldsymbol{\zeta}_2)\delta(\boldsymbol{\zeta}_1), \tag{6.4}$$

where $\hat{M}(z, \boldsymbol{\xi}, \boldsymbol{\zeta})$ is solution of

$$\begin{aligned} \frac{\partial \hat{M}}{\partial z} + \frac{i}{k_0}\boldsymbol{\xi} \cdot \boldsymbol{\zeta} \hat{M} = {} & \frac{k_0^2}{4(2\pi)^2} \int \hat{C}(\boldsymbol{k}) \Big[2\hat{M}(\boldsymbol{\xi} - \boldsymbol{k}, \boldsymbol{\zeta}) + 2\hat{M}(\boldsymbol{\xi}, \boldsymbol{\zeta} - \boldsymbol{k}) \\ & - 2\hat{M}(\boldsymbol{\xi}, \boldsymbol{\zeta}) - \hat{M}(\boldsymbol{\xi} - \boldsymbol{k}, \boldsymbol{\zeta} - \boldsymbol{k}) - \hat{M}(\boldsymbol{\xi} + \boldsymbol{k}, \boldsymbol{\zeta} - \boldsymbol{k}) \Big] d\boldsymbol{k}, \end{aligned} \tag{6.5}$$

starting from $\hat{M}(z = 0, \boldsymbol{\xi}, \boldsymbol{\zeta}) = 1$.

The solution $\hat{M}$ is the quantity that is needed to characterize the two-point statistics of the backscattered field.

Note that the integration in $\boldsymbol{x}_{\rm i}$ simplifies the dependence on $\boldsymbol{\zeta}_1$ and $\boldsymbol{\xi}_1$ due to the homogeneity of the medium fluctuations in the transverse directions. This simplification allows us next to get explicit expressions for the quantities of interest.

Proof. The Fourier transform $\hat{M}^{(2)}_{\boldsymbol{x}_{\rm i}}$ satisfies

$$\frac{\partial \hat{M}^{(2)}_{\boldsymbol{x}_{\rm i}}}{\partial z} + \frac{i}{k_0}\big(\boldsymbol{\xi}_1\cdot\boldsymbol{\zeta}_1+\boldsymbol{\xi}_2\cdot\boldsymbol{\zeta}_2\big)\hat{M}^{(2)}_{\boldsymbol{x}_{\rm i}} = \frac{k_0^2}{4(2\pi)^2}\int \hat{C}(\boldsymbol{k})\Big[\hat{M}^{(2)}_{\boldsymbol{x}_{\rm i}}(\boldsymbol{\xi}_1-\boldsymbol{k},\boldsymbol{\xi}_2-\boldsymbol{k},\boldsymbol{\zeta}_2)$$
$$+\hat{M}^{(2)}_{\boldsymbol{x}_{\rm i}}(\boldsymbol{\xi}_1-\boldsymbol{k},\boldsymbol{\xi}_2,\boldsymbol{\zeta}_2-\boldsymbol{k}) + \hat{M}^{(2)}_{\boldsymbol{x}_{\rm i}}(\boldsymbol{\xi}_1+\boldsymbol{k},\boldsymbol{\xi}_2-\boldsymbol{k},\boldsymbol{\zeta}_2) + \hat{M}^{(2)}_{\boldsymbol{x}_{\rm i}}(\boldsymbol{\xi}_1+\boldsymbol{k},\boldsymbol{\xi}_2,\boldsymbol{\zeta}_2-\boldsymbol{k})$$
$$-2\hat{M}^{(2)}_{\boldsymbol{x}_{\rm i}}(\boldsymbol{\xi}_1,\boldsymbol{\xi}_2,\boldsymbol{\zeta}_2) - \hat{M}^{(2)}_{\boldsymbol{x}_{\rm i}}(\boldsymbol{\xi}_1,\boldsymbol{\xi}_2-\boldsymbol{k},\boldsymbol{\zeta}_2-\boldsymbol{k}) - \hat{M}^{(2)}_{\boldsymbol{x}_{\rm i}}(\boldsymbol{\xi}_1,\boldsymbol{\xi}_2+\boldsymbol{k},\boldsymbol{\zeta}_2-\boldsymbol{k})\Big]d\boldsymbol{k}, \quad (6.6)$$

starting from $\hat{M}^{(2)}_{\boldsymbol{x}_{\rm i}}(z=0,\boldsymbol{\xi}_1,\boldsymbol{\xi}_2,\boldsymbol{\zeta}_1,\boldsymbol{\zeta}_2)=\exp(-2i\boldsymbol{\zeta}_1\cdot\boldsymbol{x}_{\rm i})$. Note that $\boldsymbol{\zeta}_1$ is frozen in this equation. If we denote by $\hat{M}^{(2)}_0(z,\boldsymbol{\xi}_1,\boldsymbol{\xi}_2,\boldsymbol{\zeta}_1,\boldsymbol{\zeta}_2)$ the solution with $\boldsymbol{x}_{\rm i}=\boldsymbol{0}$, then we have

$$\hat{M}^{(2)}_{\boldsymbol{x}_{\rm i}}(z,\boldsymbol{\xi}_1,\boldsymbol{\xi}_2,\boldsymbol{\zeta}_1,\boldsymbol{\zeta}_2) = \exp(-2i\boldsymbol{\zeta}_1\cdot\boldsymbol{x}_{\rm i})\hat{M}^{(2)}_0(z,\boldsymbol{\xi}_1,\boldsymbol{\xi}_2,\boldsymbol{\zeta}_1,\boldsymbol{\zeta}_2).$$

Therefore

$$\int d\boldsymbol{x}_{\rm i}\hat{M}^{(2)}_{\boldsymbol{x}_{\rm i}}(z,\boldsymbol{\xi}_1,\boldsymbol{\xi}_2,\boldsymbol{\zeta}_1,\boldsymbol{\zeta}_2) = \pi^2\hat{M}^{(2)}_0(z,\boldsymbol{\xi}_1,\boldsymbol{\xi}_2,\boldsymbol{0},\boldsymbol{\zeta}_2)\delta(\boldsymbol{\zeta}_1), \quad (6.7)$$

where $\hat{M}^{(2)}_0(z,\boldsymbol{\xi}_1,\boldsymbol{\xi}_2,\boldsymbol{0},\boldsymbol{\zeta}_2)$ is solution of

$$\frac{\partial \hat{M}^{(2)}_0}{\partial z} + \frac{i}{k_0}\boldsymbol{\xi}_2\cdot\boldsymbol{\zeta}_2\hat{M}^{(2)}_0 = \frac{k_0^2}{4(2\pi)^2}\int \hat{C}(\boldsymbol{k})\Big[\hat{M}^{(2)}_0(\boldsymbol{\xi}_1-\boldsymbol{k},\boldsymbol{\xi}_2-\boldsymbol{k},\boldsymbol{\zeta}_2)$$
$$+\hat{M}^{(2)}_0(\boldsymbol{\xi}_1-\boldsymbol{k},\boldsymbol{\xi}_2,\boldsymbol{\zeta}_2-\boldsymbol{k}) + \hat{M}^{(2)}_0(\boldsymbol{\xi}_1+\boldsymbol{k},\boldsymbol{\xi}_2-\boldsymbol{k},\boldsymbol{\zeta}_2) + \hat{M}^{(2)}_0(\boldsymbol{\xi}_1+\boldsymbol{k},\boldsymbol{\xi}_2,\boldsymbol{\zeta}_2-\boldsymbol{k})$$
$$-2\hat{M}^{(2)}_0(\boldsymbol{\xi}_1,\boldsymbol{\xi}_2,\boldsymbol{\zeta}_2) - \hat{M}^{(2)}_0(\boldsymbol{\xi}_1,\boldsymbol{\xi}_2-\boldsymbol{k},\boldsymbol{\zeta}_2-\boldsymbol{k}) - \hat{M}^{(2)}_0(\boldsymbol{\xi}_1,\boldsymbol{\xi}_2+\boldsymbol{k},\boldsymbol{\zeta}_2-\boldsymbol{k})\Big]d\boldsymbol{k},$$

starting from $\hat{M}^{(2)}_0(z=0,\boldsymbol{\xi}_1,\boldsymbol{\xi}_2,\boldsymbol{0},\boldsymbol{\zeta}_2)=1$. The solution is independent of $\boldsymbol{\xi}_1$. Therefore

$$\hat{M}^{(2)}_0(z,\boldsymbol{\xi}_1,\boldsymbol{\xi}_2,\boldsymbol{0},\boldsymbol{\zeta}_2) = \hat{M}(z,\boldsymbol{\xi}_2,\boldsymbol{\zeta}_2), \quad (6.8)$$

where $\hat{M}(z,\boldsymbol{\xi},\boldsymbol{\zeta})$ is solution of (6.5). □

7. The Covariance Function of the Backscattered Field. After substitution of (6.4) into the expression (3.4) of the covariance function of the backscattered field, and after integration in $\boldsymbol{x}_0'$ and $\boldsymbol{x}_0$, we get

$$\mathbb{E}[u(0,\boldsymbol{x}_r)\overline{u(0,\boldsymbol{x}_r')}] = \frac{\sigma^2 r_0^2}{256\pi^3}\int dz\rho(z)\int d\boldsymbol{\xi}\int d\boldsymbol{\zeta}\hat{M}(z,\boldsymbol{\xi},\boldsymbol{\zeta})$$
$$\times\exp\Big(i(\boldsymbol{x}_r'-\boldsymbol{x}_r)\cdot\boldsymbol{\xi} - i\frac{\boldsymbol{x}_r+\boldsymbol{x}_r'}{2}\cdot\boldsymbol{\zeta} - \frac{|\boldsymbol{\zeta}|^2 r_0^2}{4} - \frac{|\boldsymbol{x}_r'-\boldsymbol{x}_r|^2}{4r_0^2}\Big). \quad (7.1)$$

We then get the expression for the covariance function

$$\mathbb{E}[u(0,\boldsymbol{x}_r)\overline{u(0,\boldsymbol{x}_r')}] = \frac{\sigma^2 r_0^2}{64\pi}\int dz\rho(z)\int d\boldsymbol{\zeta}M(z,\boldsymbol{x}_r'-\boldsymbol{x}_r,\boldsymbol{\zeta})$$
$$\times\exp\Big(-i\frac{\boldsymbol{x}_r+\boldsymbol{x}_r'}{2}\cdot\boldsymbol{\zeta} - \frac{|\boldsymbol{\zeta}|^2 r_0^2}{4} - \frac{|\boldsymbol{x}_r'-\boldsymbol{x}_r|^2}{4r_0^2}\Big), \quad (7.2)$$

where $M(z,\boldsymbol{x},\boldsymbol{\zeta})$ is the inverse Fourier transform (in $\boldsymbol{\xi}$) of $\hat{M}(z,\boldsymbol{\xi},\boldsymbol{\zeta})$,

$$M(z,\boldsymbol{x},\boldsymbol{\zeta}) = \frac{1}{(2\pi)^2}\int \hat{M}(z,\boldsymbol{\xi},\boldsymbol{\zeta})\exp\big(i\boldsymbol{\xi}\cdot\boldsymbol{x}\big)d\boldsymbol{\xi},$$

and it is solution of the transport equation

$$\frac{\partial M}{\partial z} + \frac{1}{k_0}\boldsymbol{\zeta}\cdot\nabla_{\boldsymbol{x}} M = \frac{k_0^2}{(2\pi)^2}\int \hat{C}(\boldsymbol{k})\sin^2\Big(\frac{\boldsymbol{k}\cdot\boldsymbol{x}}{2}\Big)\big[M(\boldsymbol{x},\boldsymbol{\zeta}-\boldsymbol{k}) - M(\boldsymbol{x},\boldsymbol{\zeta})\big]d\boldsymbol{k}, \quad (7.3)$$

starting from $M(z=0,\boldsymbol{x},\boldsymbol{\zeta}) = \delta(\boldsymbol{x})$. Eq. (7.2) gives the general expression of the covariance function of the backscattered field in the random paraxial regime. It is naturally a function of the offset $\boldsymbol{x}_r - \boldsymbol{x}_r'$ and the mid-point $(\boldsymbol{x}_r + \boldsymbol{x}_r')/2$, and it depends on the solution M of the transport equation (7.3). The solution of the transport equation (7.3) would give the expression of the needed fourth-order moment and the covariance function of the backscattered field. However, in contrast to the second-order moment as discussed in [18], we cannot solve this equation and find a closed-form expression of the fourth-order moment in the general case. Therefore we address in the next two subsections the two particular regimes described in Section 5 in which explicit expressions can be obtained. These two regimes are very different in that the spot-dancing regime that we address in Subsection 7.1 is characterized by a large variance of the transmitted intensity distribution, while the scintillation regime that we address in Subsection 7.2 is characterized by a normalized variance of the transmitted field that stabilizes to the value one, which is characteristic of complex Gaussian fields [18]. In this derivation it will be convenient to work with the Wigner transform of the field which can be articulated directly in terms of $\hat{M}$.

7.1. Spot-Dancing Regime. The spot dancing regime was originally studied in [6]. If the covariance function is of the form (5.1), provided that $\hat{C}$ decays fast enough (so that $\int |\boldsymbol{k}|^4\hat{C}(\boldsymbol{k})d\boldsymbol{k} < \infty$), the equation (6.5) for the Fourier transform of the fourth-order moment can be simplified as $\varepsilon \to 0$:

$$\frac{\partial \hat{M}}{\partial z} + \frac{i}{k_0}\boldsymbol{\xi}\cdot\boldsymbol{\zeta}\hat{M} = 0, \quad (7.4)$$

which means that we recover the same equation as if the medium was homogeneous. This equation can be solved:

$$\hat{M}(z,\boldsymbol{\xi},\boldsymbol{\zeta}) = \exp\Big(-i\frac{z}{k_0}\boldsymbol{\xi}\cdot\boldsymbol{\zeta}\Big), \quad (7.5)$$

and after substitution into (7.1) and integration in $\boldsymbol{\xi}$ we find

$$\mathbb{E}[u(0,\boldsymbol{x}_r)\overline{u(0,\boldsymbol{x}_r')}] = \frac{\sigma^2 k_0^2 r_0^2}{64}\int dz\frac{\rho(z)}{z^2}\exp\Big(\frac{ik_0}{2z}\big(|\boldsymbol{x}_r|^2 - |\boldsymbol{x}_r'|^2\big) - \frac{1+\frac{k_0^2 r_0^4}{z^2}}{4r_0^2}|\boldsymbol{x}_r' - \boldsymbol{x}_r|^2\Big). \quad (7.6)$$

This shows that the backscattered field has a mean intensity that is independent of $\boldsymbol{x}_r$:

$$\mathbb{E}[|u(0,\boldsymbol{x}_r)|^2] = \frac{\sigma^2 k_0^2 r_0^2}{64}\int dz\frac{\rho(z)}{z^2}. \quad (7.7)$$

If we consider the Wigner transform of the backscattered field defined by

$$W_{\rm b}(\boldsymbol{x},\boldsymbol{q}) = \int \mathbb{E}\big[u(0,\boldsymbol{x}+\frac{\boldsymbol{y}}{2})\overline{u(0,\boldsymbol{x}-\frac{\boldsymbol{y}}{2})}\big]\exp\big(-i\boldsymbol{q}\cdot\boldsymbol{y}\big)d\boldsymbol{y}, \quad (7.8)$$

then we find

$$W_{\rm b}(\boldsymbol{x},\boldsymbol{q}) = \frac{\pi\sigma^2}{16}\int dz \frac{\rho(z)k_0^2 r_0^4}{z^2+k_0^2 r_0^4}\exp\Big(-\frac{|z\boldsymbol{q}-k_0\boldsymbol{x}|^2 r_0^2}{z^2+k_0^2 r_0^4}\Big). \tag{7.9}$$

The Wigner transform gives the energy flux density (in space and direction) that goes through $\boldsymbol{x}$ with the direction corresponding to the transverse wavevector $\boldsymbol{q}$ (that is, with the angle $|\boldsymbol{q}|/k_0$ compared to the normal incidence). By integrating in $\boldsymbol{q}$ we recover the mean intensity:

$$\frac{1}{(2\pi)^2}\int W_{\rm b}(\boldsymbol{x},\boldsymbol{q})d\boldsymbol{q} = \mathbb{E}[|u(0,\boldsymbol{x})|^2].$$

By looking at the Wigner transform (7.9) at $\boldsymbol{x}=\boldsymbol{0}$ as a function of $\boldsymbol{q}$, we find that the energy flux at the center has a well-defined angular profile. If the Poisson cloud of point scatterers is concentrated around the distance $z_{\rm b}$, or if we use the time-windowing technique to select the waves backscattered from the distance $z_{\rm b}$, then the energy flux density has the form of a Gaussian profile with width $Q_{\rm b}$ given by

$$Q_{\rm b}^2 = \frac{k_0^2 r_0^2}{z_{\rm b}^2} + \frac{1}{r_0^2}.$$

This angular cone can be interpreted as follows:
- if $z_{\rm b} \ll k_0 r_0^2$, then there is no diffraction and the beam width at the level of the point scatterers is r_0. This in turn, in view of the fact that the microscatterers are modeled as point scatterers, illuminates the center of the initial plane with an angular cone with opening angle of the order of $r_0/z_{\rm b}$, which corresponds to $Q_{\rm b}/k_0$.
- if $z_{\rm b} \gg k_0 r_0^2$, then there is diffraction and the beam width at the level of the point scatterers is $z_{\rm b}/(k_0 r_0)$ [18]. This in turn illuminates the center of the initial plane with an angular cone of opening angle of the order of $1/(k_0 r_0)$, which corresponds to $Q_{\rm b}/k_0$.

7.2. Scintillation Regime. We now assume the scintillation regime, that is to say, the fluctuations of the medium are small, of the order of ε, as in (5.7), the radius of the source is large, given by r_0/ε, and the propagation distance is large, of the order of ε^{-1}, with the density of the Poisson cloud of the form $\varepsilon\rho(\varepsilon z)$. Then (7.1) reads (for any $\varepsilon > 0$)

$$\begin{aligned}\mathbb{E}[u(0,\boldsymbol{x}_r)\overline{u(0,\boldsymbol{x}_r')}] = \frac{\sigma^2 r_0^2}{256\pi^2\varepsilon^2}\int dz\rho(z)\int d\boldsymbol{\xi}\int d\boldsymbol{\zeta}\hat{M}\big(\frac{z}{\varepsilon},\boldsymbol{\xi},\boldsymbol{\zeta}\big)\\ \times\exp\Big(i(\boldsymbol{x}_r'-\boldsymbol{x}_r)\cdot\boldsymbol{\xi} - i\frac{\boldsymbol{x}_r+\boldsymbol{x}_r'}{2}\cdot\boldsymbol{\zeta} - \frac{|\boldsymbol{\zeta}|^2 r_0^2}{4\varepsilon^2} - \frac{\varepsilon^2|\boldsymbol{x}_r'-\boldsymbol{x}_r|^2}{4r_0^2}\Big).\end{aligned} \tag{7.10}$$

The covariance function depends on a scaled version of the fourth-order moment $\hat{M}$. Let us introduce the new function $\tilde{M}^\varepsilon$ defined by

$$\tilde{M}^\varepsilon(z,\boldsymbol{\xi},\boldsymbol{\zeta}) = \hat{M}\big(\frac{z}{\varepsilon},\boldsymbol{\xi},\boldsymbol{\zeta}\big)\exp\Big(i\frac{z}{\varepsilon k_0}\boldsymbol{\xi}\cdot\boldsymbol{\zeta}\Big) \tag{7.11}$$

that satisfies

$$\begin{aligned}\frac{\partial\tilde{M}^\varepsilon}{\partial z} = \frac{k_0^2}{4(2\pi)^2}\int\hat{C}(\boldsymbol{k})\Big[2\tilde{M}^\varepsilon(\boldsymbol{\xi}-\boldsymbol{k},\boldsymbol{\zeta})e^{i\frac{z}{\varepsilon k_0}\boldsymbol{k}\cdot\boldsymbol{\zeta}} + 2\tilde{M}^\varepsilon(\boldsymbol{\xi},\boldsymbol{\zeta}-\boldsymbol{k})e^{i\frac{z}{\varepsilon k_0}\boldsymbol{k}\cdot\boldsymbol{\xi}} - 2\tilde{M}^\varepsilon(\boldsymbol{\xi},\boldsymbol{\zeta})\\ -\tilde{M}^\varepsilon(\boldsymbol{\xi}-\boldsymbol{k},\boldsymbol{\zeta}-\boldsymbol{k})e^{i\frac{z}{\varepsilon k_0}(\boldsymbol{k}\cdot(\boldsymbol{\xi}+\boldsymbol{\zeta})-|\boldsymbol{k}|^2)} - \tilde{M}^\varepsilon(\boldsymbol{\xi}+\boldsymbol{k},\boldsymbol{\zeta}-\boldsymbol{k})e^{i\frac{z}{\varepsilon k_0}(\boldsymbol{k}\cdot(\boldsymbol{\xi}-\boldsymbol{\zeta})+|\boldsymbol{k}|^2)}\Big]d\boldsymbol{k},\end{aligned} \tag{7.12}$$

starting from $\tilde{M}^\varepsilon(z=0,\boldsymbol{\xi},\boldsymbol{\zeta})=1$. The function $\tilde{M}^\varepsilon$ has a multi-scale behavior as $\varepsilon\to 0$ as explained in the following proposition, which originates from the averaging of the rapid phases in (7.12).

PROPOSITION 7.1. *For any $Z>0$, we have*

$$\sup_{z\in[0,Z],\boldsymbol{\xi},\boldsymbol{\zeta}\in\mathbb{R}^2}\Big|\tilde{M}^\varepsilon(z,\boldsymbol{\xi},\boldsymbol{\zeta})-\tilde{M}^0\big(z,\frac{\boldsymbol{\zeta}}{\varepsilon}\big)-\tilde{M}^0\big(z,\frac{\boldsymbol{\xi}}{\varepsilon}\big)+\exp\big(-\frac{k_0^2C(\mathbf{0})z}{2}\big)\Big|\overset{\varepsilon\to 0}{\longrightarrow}0, \quad (7.13)$$

where

$$\tilde{M}^0(z,\boldsymbol{\zeta})=\exp\Big(\frac{k_0^2}{2}\int_0^z C\big(\frac{z'}{k_0}\boldsymbol{\zeta}\big)-C(\mathbf{0})dz'\Big). \quad (7.14)$$

This means that:

1. *As $\varepsilon\to 0$, we have $\tilde{M}^\varepsilon(z,\boldsymbol{\xi},\boldsymbol{\zeta})\to\exp(-\frac{k_0^2C(\mathbf{0})z}{2})$ for any $\boldsymbol{\xi},\boldsymbol{\zeta}\neq 0$.*
2. *As $\varepsilon\to 0$, we have $\tilde{M}^\varepsilon(z,\boldsymbol{\xi},\varepsilon\boldsymbol{\zeta})\to\tilde{M}^0(z,\boldsymbol{\zeta})$ for any $\boldsymbol{\xi}\neq 0$.*
3. *As $\varepsilon\to 0$, we have $\tilde{M}^\varepsilon(z,\varepsilon\boldsymbol{\xi},\boldsymbol{\zeta})\to\tilde{M}^0(z,\boldsymbol{\xi})$ for any $\boldsymbol{\zeta}\neq 0$.*
4. *As $\varepsilon\to 0$, we have $\tilde{M}^\varepsilon(z,\varepsilon\boldsymbol{\xi},\varepsilon\boldsymbol{\zeta})\to\tilde{M}^0(z,\boldsymbol{\zeta})+\tilde{M}^0(z,\boldsymbol{\xi})-\exp(-\frac{k_0^2C(\mathbf{0})z}{2})$ for any $\boldsymbol{\xi},\boldsymbol{\zeta}$.*

Proof. Here we give a rapid and formal proof. We give in the appendix a complete and detailed proof. In case *(1)*, the rapid phases cancel the contributions of all but the term $-2\tilde{M}^\varepsilon(\boldsymbol{\xi},\boldsymbol{\zeta})$ in (7.12), and we get in the limit $\varepsilon\to 0$ that $\tilde{M}(z,\boldsymbol{\xi},\boldsymbol{\zeta})=\lim_{\varepsilon\to 0}\tilde{M}^\varepsilon(z,\boldsymbol{\xi},\boldsymbol{\zeta})$ satisfies:

$$\frac{\partial\tilde{M}}{\partial z}=-\frac{k_0^2}{2(2\pi)^2}\int\hat{C}(\boldsymbol{k})\tilde{M}d\boldsymbol{k}=-\frac{k_0^2}{2}C(\mathbf{0})\tilde{M},$$

which gives the first result. In case *(2)*, we obtain in the limit $\varepsilon\to 0$ the simplified system for $\tilde{M}(z,\boldsymbol{\xi},\boldsymbol{\zeta})=\lim_{\varepsilon\to 0}\tilde{M}^\varepsilon(z,\boldsymbol{\xi},\varepsilon\boldsymbol{\zeta})$:

$$\frac{\partial\tilde{M}}{\partial z}=\frac{k_0^2}{2(2\pi)^2}\int\hat{C}(\boldsymbol{k})\big[\tilde{M}(\boldsymbol{\xi}-\boldsymbol{k},\boldsymbol{\zeta})e^{i\frac{z}{k_0}\boldsymbol{k}\cdot\boldsymbol{\zeta}}-\tilde{M}(\boldsymbol{\xi},\boldsymbol{\zeta})\big]d\boldsymbol{k}.$$

We obtain that the solution does not depend on $\boldsymbol{\xi}$ and that it is given by (7.14). Case *(3)* is similar.

In case *(4)* we obtain the simplified system for $\tilde{M}(z,\boldsymbol{\xi},\boldsymbol{\zeta})=\lim_{\varepsilon\to 0}\tilde{M}^\varepsilon(z,\varepsilon\boldsymbol{\xi},\varepsilon\boldsymbol{\zeta})$:

$$\frac{\partial\tilde{M}}{\partial z}=\frac{k_0^2}{2(2\pi)^2}\int\hat{C}(\boldsymbol{k})\big[\tilde{M}^0(\boldsymbol{\zeta})e^{i\frac{z}{k_0}\boldsymbol{k}\cdot\boldsymbol{\zeta}}+\tilde{M}^0(\boldsymbol{\xi})e^{i\frac{z}{k_0}\boldsymbol{k}\cdot\boldsymbol{\xi}}-\tilde{M}(\boldsymbol{\xi},\boldsymbol{\zeta})\big]d\boldsymbol{k}.$$

Using the equation satisfied by $\tilde{M}_0$, we get

$$\frac{\partial\tilde{M}(\boldsymbol{\xi},\boldsymbol{\zeta})}{\partial z}=\frac{\partial\tilde{M}^0(\boldsymbol{\zeta})}{\partial z}+\frac{\partial\tilde{M}^0(\boldsymbol{\xi})}{\partial z}+\frac{k_0^2}{2}C(\mathbf{0})\big[\tilde{M}^0(\boldsymbol{\zeta})+\tilde{M}^0(\boldsymbol{\xi})-\tilde{M}(\boldsymbol{\xi},\boldsymbol{\zeta})\big],$$

which yields the desired result. □

The scaled Wigner transform of the backscattered field is defined by

$$W_{\rm b}(\boldsymbol{x},\boldsymbol{q})=\frac{1}{\varepsilon^2}\int\mathbb{E}\big[u(0,\frac{\boldsymbol{x}}{\varepsilon}+\frac{\boldsymbol{y}}{2\varepsilon})\overline{u(0,\frac{\boldsymbol{x}}{\varepsilon}-\frac{\boldsymbol{y}}{2\varepsilon})}\big]\exp\big(-i\boldsymbol{q}\cdot\frac{\boldsymbol{y}}{\varepsilon}\big)d\boldsymbol{y}. \quad (7.15)$$

Note that we observe the backscattered field at the scale $1/\varepsilon$ corresponding to the original beam width. The following proposition describes the multiscale behavior of the Wigner transform of the backscattered field.

PROPOSITION 7.2. *In the scintillation regime $\varepsilon \to 0$ the Wigner transform of the backscattered field satisfies the two following identities:*
1) For $\boldsymbol{q} \neq \boldsymbol{0}$:

$$W_{\rm b}(\boldsymbol{x},\boldsymbol{q}) \stackrel{\varepsilon\to 0}{=} \frac{\sigma^2 r_0^2}{64}\int dz\rho(z)\int d\boldsymbol{\zeta}\tilde{M}^0(z,\boldsymbol{\zeta})\exp\Big(-i\boldsymbol{\zeta}\cdot\big(\boldsymbol{x}-\boldsymbol{q}\frac{z}{k_0}\big)-\frac{|\boldsymbol{\zeta}|^2 r_0^2}{4}\Big), \quad (7.16)$$

where $\tilde{M}^0$ is defined by (7.14).
2) For any $\boldsymbol{q}$:

$$W_{\rm b}(\boldsymbol{x},\varepsilon\boldsymbol{q}) \stackrel{\varepsilon\to 0}{=} \frac{\sigma^2 r_0^4}{64\pi}\int dz\rho(z)\iint d\boldsymbol{\xi}d\boldsymbol{\zeta}\Big[\tilde{M}^0(z,\boldsymbol{\xi}-\boldsymbol{q})+\tilde{M}^0(z,\boldsymbol{\zeta})-\exp\big(-\frac{k_0^2 C(\boldsymbol{0})z}{2}\big)\Big]$$
$$\times\exp\Big(-i\boldsymbol{x}\cdot\boldsymbol{\zeta}-\frac{|\boldsymbol{\zeta}|^2 r_0^2}{4}-r_0^2|\boldsymbol{\xi}|^2\Big). \quad (7.17)$$

Proof. We find from (7.10) after integration in $\boldsymbol{y}$:

$$W_{\rm b}(\boldsymbol{x},\boldsymbol{q}) = \frac{\sigma^2 r_0^4}{64\pi}\int dz\rho(z)\iint d\boldsymbol{\xi}d\boldsymbol{\zeta}\hat{M}\big(\frac{z}{\varepsilon},\varepsilon\boldsymbol{\xi}-\boldsymbol{q},\varepsilon\boldsymbol{\zeta}\big)$$
$$\times\exp\Big(-i\boldsymbol{x}\cdot\boldsymbol{\zeta}-\frac{|\boldsymbol{\zeta}|^2 r_0^2}{4}-r_0^2|\boldsymbol{\xi}|^2\Big). \quad (7.18)$$

We can then get (7.16) from (7.18) and Proposition 7.1 (item 2). We can also get (7.17) from (7.18) and Proposition 7.1 (item 4). □

The two closed-form expressions (7.16-7.17) will be discussed in more detail in the following. They show that the Wigner transform has a multiscale behavior in $\boldsymbol{q}$: Eq. (7.16) gives the behavior for angles of order one (that are not zero), and Eq. (7.17) gives the behavior for small angles of order ε. We can check that, in the asymptotics $\varepsilon \to 0$, the limit of $W_{\rm b}(\boldsymbol{x},\varepsilon\boldsymbol{q})$ for large $\boldsymbol{q}$ is equivalent to the limit of $W_{\rm b}(\boldsymbol{x},\boldsymbol{q})$ for small $\boldsymbol{q}$. This means that, as a function of $\boldsymbol{q}$, (7.17) can be seen as a peak of width of order ε on the top of a profile of width of order one described by (7.16).

We can remark by integrating in $\boldsymbol{q}$ that

$$\mathbb{E}\big[|u(0,\frac{\boldsymbol{x}}{\varepsilon})|^2\big] \stackrel{\varepsilon\to 0}{=} \frac{\sigma^2 k_0^2 r_0^2}{64}\int dz\frac{\rho(z)}{z^2}, \quad (7.19)$$

which is independent on the fluctuations of the random medium and is equal to the mean intensity of the backscattered field in the homogeneous case (see (7.7)). This shows that the effects of the random medium can only be felt at the level of the correlations of the backscattered field, or equivalently at the level of the Wigner transform, and not at the level of the mean backscattered intensity.

Finally, if we denote

$$\hat{u}(0,\boldsymbol{q}) = \int u(0,\boldsymbol{x})\exp\big(-i\boldsymbol{q}\cdot\boldsymbol{x}\big)d\boldsymbol{x},$$

and introduce the total energy flux density $\mathbb{E}[|\hat{u}(0,\boldsymbol{q})|^2]$ that can also be computed from the Wigner transform by integrating in $\boldsymbol{x}$:

$$\varepsilon^2\mathbb{E}[|\hat{u}(0,\boldsymbol{q})|^2] = \int W_{\rm b}(\boldsymbol{x},\boldsymbol{q})d\boldsymbol{x},$$

then we have for any $\boldsymbol{q} \neq \mathbf{0}$:

$$\varepsilon^2 \mathbb{E}[|\hat{u}(0,\boldsymbol{q})|^2] \stackrel{\varepsilon \to 0}{=} \frac{\pi^2 \sigma^2 r_0^2}{16} \int dz \rho(z), \tag{7.20}$$

and for any $\boldsymbol{q}$:

$$\varepsilon^2 \mathbb{E}[|\hat{u}(0,\varepsilon\boldsymbol{q})|^2] \stackrel{\varepsilon \to 0}{=} \frac{\pi^2 \sigma^2 r_0^2}{16} \int dz \rho(z) \Big[1 - \exp\big(- \frac{k_0^2 C(\mathbf{0}) z}{2} \big) + \tilde{E}(z,\boldsymbol{q}) \Big], \tag{7.21}$$

with

$$\tilde{E}(z,\boldsymbol{q}) = \frac{r_0^2}{\pi} \int \tilde{M}^0(z, \boldsymbol{\xi} - \boldsymbol{q}) \exp\big(- r_0^2 |\boldsymbol{\xi}|^2 \big) d\boldsymbol{\xi}.$$

The last term $\tilde{E}(z,\boldsymbol{q})$ indicates that the total energy flux density has a flat background but with an additional narrow peak around the normal (or backscattered) direction $\boldsymbol{q} = \mathbf{0}$. If the Poisson cloud of point scatterers is concentrated around the distance $z_{\rm b}$, or if we use the time-windowing technique to select the waves backscattered from the distance $z_{\rm b}$, then the relative amplitude of the cone is

$$A_{\rm b} = 1 - \exp\big(- \frac{k_0^2 C(\mathbf{0}) z_{\rm b}}{2} \big) + \frac{r_0^2}{\pi} \int \tilde{M}^0(z_{\rm b}, \boldsymbol{\xi}) \exp\big(- r_0^2 |\boldsymbol{\xi}|^2 \big) d\boldsymbol{\xi}.$$

We discuss the shape of the cone in detail in the next section.

8. The Wigner Distribution of the Backscattered Field in the Scintillation Regime.

8.1. Weakly Scattering Media. If $k_0^2 C(\mathbf{0}) z \ll 1$, then $\tilde{M}^0(z,\boldsymbol{\xi}) = 1$ for any $\boldsymbol{\xi}$. From (7.16) we get then the same results as in the homogeneous case with scintillation scaling. The Wigner distribution of the backscattered field (7.15) is of the form

$$W_{\rm b}(\boldsymbol{x},\boldsymbol{q}) \stackrel{\varepsilon \to 0}{=} \frac{\pi \sigma^2}{16} \int dz \rho(z) \exp\Big(- \frac{|\boldsymbol{x} - \boldsymbol{q} \frac{z}{k_0}|^2}{r_0^2} \Big). \tag{8.1}$$

This expression is valid for large angles, when $|\boldsymbol{q}|$ is of order one. For small angles, corresponding to a small transverse wavevector $\varepsilon\boldsymbol{q}$, we find from (7.17)

$$W_{\rm b}(\boldsymbol{x},\varepsilon\boldsymbol{q}) \stackrel{\varepsilon \to 0}{=} \frac{\pi \sigma^2}{16} \int dz \rho(z) \exp\Big(- \frac{|\boldsymbol{x}|^2}{r_0^2} \Big), \tag{8.2}$$

which is here the limit of (8.1) as $\boldsymbol{q} \to \mathbf{0}$. This shows that there is no multiscale behavior in this regime. If the Poisson cloud of point scatterers is concentrated around the distance $z_{\rm b}$, or if we use the time-windowing technique to select the waves backscattered from the distance $z_{\rm b}$, then the energy flux density received at the center $\boldsymbol{x} = \mathbf{0}$ has the form of a Gaussian profile with width $Q_{\rm b}$ given by

$$Q_{\rm b} = \frac{k_0 r_0}{z_{\rm b}}.$$

This angular cone can be interpreted as at the end of Section 7.1 (here the width of the initial beam is large and the propagation distance is smaller than the Rayleigh distance).

8.2. Strongly Scattering Smooth Media. If $k_0^2 C(\mathbf{0}) z \gg 1$, and if, additionally, C is smooth and we can use (5.2), then $C(\boldsymbol{x})$ can be expanded as $C(\boldsymbol{x}) = C(\mathbf{0}) - \gamma|\boldsymbol{x}|^2/2 + o(|\boldsymbol{x}|^2)$ and (7.14) can be expanded as

$$\tilde{M}^0(z,\boldsymbol{\xi}) = \exp\Big(-\frac{\gamma z^3}{12}|\boldsymbol{\xi}|^2\Big). \tag{8.3}$$

For $\boldsymbol{q} \neq \mathbf{0}$ this gives after substitution in (7.16) and after integration in $\boldsymbol{\zeta}$:

$$W_{\rm b}(\boldsymbol{x},\boldsymbol{q}) \stackrel{\varepsilon\to 0}{=} \frac{\pi\sigma^2 r_0^2}{16}\int dz\rho(z)\frac{1}{r_0^2+\frac{\gamma z^3}{3}}\exp\Big(-\frac{|\boldsymbol{x}-\boldsymbol{q}\frac{z}{k_0}|^2}{r_0^2+\frac{\gamma z^3}{3}}\Big). \tag{8.4}$$

For the following discussion, we will assume that the Poisson cloud is concentrated at some distance $z_{\rm b}$, or that we use the time-windowing technique to select the waves backscattered from the distance $z_{\rm b}$. The Wigner transform $W_{\rm b}(\boldsymbol{x}=\mathbf{0},\boldsymbol{q})$ measures the backscattered energy flux at the center in the direction corresponding to the transverse wavevector $\boldsymbol{q}$, that is, with the angle $|\boldsymbol{q}|/k_0$. By looking at the expression (8.4) at $\boldsymbol{x}=\mathbf{0}$:

$$W_{\rm b}(\mathbf{0},\boldsymbol{q}) \stackrel{\varepsilon\to 0}{=} \frac{\pi\sigma^2 r_0^2}{16(r_0^2+\frac{\gamma z_{\rm b}^3}{3})}\Big[\int dz\rho(z)\Big]\exp\Big(-\frac{|\boldsymbol{q}|^2}{\frac{k_0^2 r_0^2}{z_{\rm b}^2}+\frac{\gamma k_0^2 z_{\rm b}}{3}}\Big), \tag{8.5}$$

we find that the energy flux density has the form of a broad Gaussian profile with width $Q_{\rm b}$ given by

$$Q_{\rm b}^2 = \frac{k_0^2 r_0^2}{z_{\rm b}^2}+\frac{\gamma k_0^2 z_{\rm b}}{3}.$$

Using the fact that the beam width at the level of the point scatterers is $\sqrt{r_0^2+\gamma z_{\rm b}^3/6}$ [17, Eq. (63)], this angular cone can be interpreted as follows:
- if $\gamma z_{\rm b}^3 \ll r_0^2$, then the beam width at the level of the point scatterers is r_0. This in turn illuminates the initial plane with an angular cone of width of the order of $r_0/z_{\rm b}$, which corresponds to $Q_{\rm b}/k_0$.
- if $\gamma z_{\rm b}^3 \gg r_0^2$, then the beam width at the level of the point scatterers is $\gamma^{1/2} z_{\rm b}^{3/2}$. This in turn illuminates the initial plane with an angular cone of width of the order of $\gamma^{1/2} z_{\rm b}^{1/2}$, which corresponds to $Q_{\rm b}/k_0$.

The expression (8.4) is valid when $|\boldsymbol{q}|$ is of order one. For small transverse wavevector $\varepsilon\boldsymbol{q}$ we get from (7.17) and after integration in $\boldsymbol{\zeta},\boldsymbol{\xi}$ that

$$\begin{aligned} W_{\rm b}(\boldsymbol{x},\varepsilon\boldsymbol{q}) \stackrel{\varepsilon\to 0}{=} \frac{\pi\sigma^2 r_0^2}{16}\int dz\rho(z)\Big[&\frac{1}{r_0^2+\frac{\gamma z^3}{3}}\exp\Big(-\frac{|\boldsymbol{x}|^2}{r_0^2+\frac{\gamma z^3}{3}}\Big) \\ &+\frac{1}{r_0^2+\frac{\gamma z^3}{12}}\exp\Big(-\frac{|\boldsymbol{x}|^2}{r_0^2}-\frac{|\boldsymbol{q}|^2 r_0^2\frac{\gamma z^3}{12}}{r_0^2+\frac{\gamma z^3}{12}}\Big)\Big]. \end{aligned} \tag{8.6}$$

If the Poisson cloud is concentrated at some distance $z_{\rm b}$, or if we use the time-windowing technique to select the waves backscattered from the distance $z_{\rm b}$, then the directional energy flux density at the center is:

$$W_{\rm b}(\mathbf{0},\varepsilon\boldsymbol{q}) \stackrel{\varepsilon\to 0}{=} \frac{\pi\sigma^2 r_0^2}{16(r_0^2+\frac{\gamma z_{\rm b}^3}{3})}\Big[\int dz\rho(z)\Big]\Big[1+\frac{r_0^2+\frac{\gamma z_{\rm b}^3}{3}}{r_0^2+\frac{\gamma z_{\rm b}^3}{12}}\exp\Big(-\frac{|\boldsymbol{q}|^2 r_0^2\frac{\gamma z_{\rm b}^3}{12}}{r_0^2+\frac{\gamma z_{\rm b}^3}{12}}\Big)\Big]. \tag{8.7}$$

This shows that on the top of the broad Gaussian profile described by (8.5) there is in the vicinity of the normal direction, i.e. around $\boldsymbol{q} = \mathbf{0}$, an additional peak with the width $\varepsilon q_{\rm b}$ and with the enhancement factor $A_{\rm b}$ where

$$q_{\rm b}^2 = \frac{1}{r_0^2} + \frac{12}{\gamma z_{\rm b}^3}, \tag{8.8}$$

$$A_{\rm b} = 1 + \frac{r_0^2 + \frac{\gamma z_{\rm b}^3}{3}}{r_0^2 + \frac{\gamma z_{\rm b}^3}{12}}. \tag{8.9}$$

This is a manifestation of the enhanced backscattering phenomenon that has been reported in many situations in the literature [33]. However the situation is special here because we address a regime in which the waves experience single scattering by the point scatterers. The classical enhanced backscattering phenomenon happens in a regime of multiple scattering by point scatterers and it results from the constructive interference of reciprocal light paths. Here the enhanced backscattering phenomenon happens because of relatively strong scattering by the medium in the scintillation regime.

The width of the enhanced backscattering cone $q_{\rm b}$ decreases and the enhancement factor $A_{\rm b}$ increases with scattering. The enhancement factor goes from the value 2 for $\gamma z_{\rm b}^3 r_0^{-2} \ll 1$ (which corresponds to a quasi-plane wave illumination) to the value 5 for $\gamma z_{\rm b}^3 r_0^{-2} \gg 1$ and the width of the enhanced backscattering cone goes from $\gamma^{-1/2} z_{\rm b}^{-3/2}$ for $\gamma z_{\rm b}^3 r_0^{-2} \ll 1$ to the value $1/r_0$ for $\gamma z_{\rm b}^3 r_0^{-2} \gg 1$. The enhanced backscattering cone is noticeable not only at the center $\boldsymbol{x} = \mathbf{0}$ but everywhere in the quasi-planar illumination case $\gamma z_{\rm b}^3 r_0^{-2} \ll 1$. The situation is more complicated in the case $\gamma z_{\rm b}^3 r_0^{-2} \gg 1$ because the beam spreads out as it propagates due to scattering, and enhanced backscattering for the energy flux density happens only within the original beam support (hence the term $\exp(-|\boldsymbol{x}|^2/r_0^2)$ in (8.6)). If we integrate over the full backscattered beam, then the enhancement factor is smaller. More exactly, the total energy flux density $\mathbb{E}[|\hat{u}(0, \varepsilon \boldsymbol{q})|^2]$ is of the form

$$\varepsilon^2 \mathbb{E}[|\hat{u}(0, \varepsilon \boldsymbol{q})|^2] \stackrel{\varepsilon \to 0}{=} \frac{\pi^2 \sigma^2 r_0^2}{16} \Big[\int dz \rho(z) \Big] \Big[1 + \frac{r_0^2}{r_0^2 + \frac{\gamma z_{\rm b}^3}{12}} \exp\Big(- \frac{|\boldsymbol{q}|^2 r_0^2 \frac{\gamma z_{\rm b}^3}{12}}{r_0^2 + \frac{\gamma z_{\rm b}^3}{12}} \Big) \Big]. \tag{8.10}$$

We find that the enhancement factor for the total energy flux density $\mathbb{E}[|\hat{u}(0, \varepsilon \boldsymbol{q})|^2]$ is

$$A_{\rm b} = 1 + \frac{r_0^2}{r_0^2 + \frac{\gamma z_{\rm b}^3}{12}}, \tag{8.11}$$

while the width of the cone is still (8.8).

It should be noted that the fact that the density of point scatterers is invariant in the transverse direction plays an important role. The enhanced backscattering phenomenon in the case of a single point scatterer turns out to be quite different [5]. It can also be remarked that the enhanced backscattering phenomenon by a quasi-plane wave from a diffusive planar reflector in the scintillation regime gives the same result as the one obtained here (taking the limit $r_0 \to \infty$ in (8.10)), that is to say, the amplitude factor of the enhanced backscattering cone is 2 and the width of the enhanced backscattering cone is proportional to $\gamma^{-1/2} z_{\rm b}^{-3/2}$ [7]. In fact, it is shown in [7] that the relative magnitude and width of the cone are not affected by the replacement of the specular interface with a diffusive interface. We confirm here

this observation and we can also observe that when we use a beam rather than a plane wave, then the non-homogeneity of the illumination gives rise to an anomalous enhancement factor and an anomalous cone width (8.8-8.11).
An important feature of the formulas (8.8-8.11) is that they do not depend on the carrier frequency. Therefore, by using several frequencies to get statistical stability, the measurement of the width and amplitude of the spectral cone can give access to the parameter γ of the medium.

8.3. Strongly Scattering Rough Media. If $k_0^2 C(\mathbf{0}) z \gg 1$, and if, additionally, C is not smooth but can be expanded as

$$C(\boldsymbol{x}) = C(\mathbf{0}) - \frac{\gamma_H}{2}|\boldsymbol{x}|^{2H} + o(|\boldsymbol{x}|^{2H}), \tag{8.12}$$

where $H \in (0,1]$ and $\gamma_H > 0$, then for large z so that $k_0^2 C(\mathbf{0}) z \gg 1$,

$$\tilde{M}^0(z,\boldsymbol{\xi}) = \exp\big(-\alpha_H(z)|\boldsymbol{\xi}|^{2H}\big), \qquad \alpha_H(z) = \frac{\gamma_H k_0^{2(1-H)} z^{1+2H}}{4(1+2H)}. \tag{8.13}$$

For $\boldsymbol{q} \neq \mathbf{0}$ this gives after substitution in (7.16) and after integration in $\boldsymbol{\zeta}$:

$$W_{\rm b}(\boldsymbol{x},\boldsymbol{q}) \stackrel{\varepsilon\to 0}{=} \frac{\sigma^2 r_0^2}{64}\int dz \rho(z) \Phi_H\big(\boldsymbol{x} - \boldsymbol{q}\frac{z}{k_0}, z\big), \tag{8.14}$$

where

$$\Phi_H(\boldsymbol{x},z) = \int d\boldsymbol{\zeta} \exp\Big(-\frac{r_0^2|\boldsymbol{\zeta}|^2}{4} - i\boldsymbol{\zeta}\cdot\boldsymbol{x} - \alpha_H(z)|\boldsymbol{\zeta}|^{2H}\Big). \tag{8.15}$$

If $\alpha_H(z) r_0^{-2H} \ll 1$, then

$$W_{\rm b}(\boldsymbol{x},\boldsymbol{q}) \stackrel{\varepsilon\to 0}{=} \frac{\sigma^2\pi}{16}\int dz \rho(z) \exp\Big(-\frac{|\boldsymbol{x} - \boldsymbol{q}\frac{z}{k_0}|^2}{r_0^2}\Big). \tag{8.16}$$

If $\alpha_H(z) r_0^{-2H} \gg 1$, then

$$W_{\rm b}(\boldsymbol{x},\boldsymbol{q}) \stackrel{\varepsilon\to 0}{=} \frac{\sigma^2 r_0^2}{64}\int dz \frac{\rho(z)}{\alpha_H(z)^{1/H}} \Phi_H^\infty\Big(\frac{\boldsymbol{x} - \boldsymbol{q}\frac{z}{k_0}}{\alpha_H(z)^{1/(2H)}}\Big), \tag{8.17}$$

with

$$\begin{aligned}\Phi_H^\infty(\boldsymbol{v}) &= \int \exp(-|\boldsymbol{u}|^{2H} - i\boldsymbol{u}\cdot\boldsymbol{v}) d\boldsymbol{u} \\ &= 2\pi\int_0^\infty \exp(-r^{2H}) J_0(r|\boldsymbol{v}|) r dr.\end{aligned} \tag{8.18}$$

For instance, for $H = 1$ and $H = 1/2$, we have [19, formula 6.623]

$$\Phi_1^\infty(\boldsymbol{v}) = \pi\exp\big(-\frac{|\boldsymbol{v}|^2}{4}\big), \qquad \Phi_{1/2}^\infty(\boldsymbol{v}) = \frac{2\pi}{(1+|\boldsymbol{v}|^2)^{3/2}},$$

and $\Phi_H^\infty(\mathbf{0}) = \pi/H \int_0^\infty r^{-1+1/H}\exp(-r) dr = \pi\Gamma(1/H)/H$ (with Γ the Euler Gamma function).

The expression (8.14) is valid when $|\boldsymbol{q}|$ is of order one. For small transverse wavevector $\varepsilon\boldsymbol{q}$ we get from (7.17) and after integration in $\boldsymbol{\zeta}, \boldsymbol{\xi}$ that:

$$W_{\rm b}(\boldsymbol{x}, \varepsilon\boldsymbol{q}) \stackrel{\varepsilon\to 0}{=} \frac{\sigma^2 r_0^2}{64} \int dz \rho(z) \Big[\exp\Big(- \frac{|\boldsymbol{x}|^2}{r_0^2}\Big) \Psi_H(\boldsymbol{q}, z) + \Phi_H(\boldsymbol{x}, z)\Big], \tag{8.19}$$

with

$$\Psi_H(\boldsymbol{q}, z) = 4 \int d\boldsymbol{\xi} \exp\Big(- r_0^2 |\boldsymbol{\xi}|^2 - \alpha_H(z) |\boldsymbol{q} - \boldsymbol{\xi}|^{2H}\Big). \tag{8.20}$$

If we consider the backscattered energy flux at the center in the direction corresponding to the transverse wavevector $\boldsymbol{q} \neq \boldsymbol{0}$, then we find using (8.14) a broad profile

$$W_{\rm b}(\boldsymbol{0}, \boldsymbol{q}) \stackrel{\varepsilon\to 0}{=} \frac{\sigma^2 r_0^2}{64} \int dz \rho(z) \Phi_H(\frac{\boldsymbol{q} z}{k_0}, z), \tag{8.21}$$

and on the top of the broad profile exhibited by (8.21) there is an additional narrow peak centered at the normal direction $\boldsymbol{q} = \boldsymbol{0}$:

$$W_{\rm b}(\boldsymbol{0}, \varepsilon\boldsymbol{q}) \stackrel{\varepsilon\to 0}{=} \frac{\sigma^2 r_0^2}{64} \int dz \rho(z) \Phi_H(\boldsymbol{0}, z) \Big[1 + \frac{\Psi_H(\boldsymbol{q}, z)}{\Phi_H(\boldsymbol{0}, z)}\Big]. \tag{8.22}$$

If the Poisson cloud is concentrated at some distance $z_{\rm b}$, or if we use the time-windowing technique to select the waves backscattered from the distance $z_{\rm b}$, then the width of the broad profile is

$$Q_{\rm b} = \begin{cases} \dfrac{k_0 r_0}{z_{\rm b}}, & \text{if } \alpha_H(z) r_0^{-2H} \ll 1, \\ \dfrac{k_0 \alpha_H(z_{\rm b})^{1/(2H)}}{z_{\rm b}}, & \text{if } \alpha_H(z) r_0^{-2H} \gg 1. \end{cases}$$

The width $\varepsilon q_{\rm b}$ of the enhanced backscattering cone is given by the width of the function $\boldsymbol{q} \to \Psi_H(\boldsymbol{q}, z_{\rm b})$ and the enhanced backscattering amplitude factor is $A_{\rm b} = 1 + \Psi_H(\boldsymbol{0}, z_{\rm b})/\Phi_H(\boldsymbol{0}, z_{\rm b})$, which is a function of $\alpha_H(z_{\rm b}) r_0^{-2H}$ only:

$$A_{\rm b} = 1 + \frac{4 \int d\boldsymbol{u} \exp\big(- |\boldsymbol{u}|^2 - \alpha_H(z_{\rm b}) r_0^{-2H} |\boldsymbol{u}|^{2H}\big)}{\int d\boldsymbol{u} \exp\big(- |\boldsymbol{u}|^2/4 - \alpha_H(z_{\rm b}) r_0^{-2H} |\boldsymbol{u}|^{2H}\big)}.$$

If $\alpha_H(z_{\rm b}) r_0^{-2H} \ll 1$, then

$$W_{\rm b}(\boldsymbol{x}, \varepsilon\boldsymbol{q}) \stackrel{\varepsilon\to 0}{=} \frac{\sigma^2 \pi}{16} \Big[\int dz \rho(z)\Big] \Big[1 + \exp\big(- \alpha_H(z_{\rm b}) |\boldsymbol{q}|^{2H}\big)\Big] \exp\Big(- \frac{|\boldsymbol{x}|^2}{r_0^2}\Big). \tag{8.23}$$

This shows that the width of the enhanced backscattering cone is $\varepsilon q_{\rm b}$ with

$$q_{\rm b} = \frac{1}{\alpha_H(z_{\rm b})^{1/(2H)}},$$

and the enhancement factor is $A_{\rm b} = 2$. Note that this corresponds to an angular cone of $q_{\rm b}\lambda_0/(2\pi)$ that is proportional to $\lambda_0^{1/H}$, which is an anomalous frequency-behavior of the angular width of the enhanced backscattering cone that characterizes

the roughness of the fluctuations of the medium.
If $\alpha_H(z_{\rm b})r_0^{-2H} \gg 1$, then

$$W_{\rm b}(\boldsymbol{x},\varepsilon\boldsymbol{q}) \stackrel{\varepsilon\to 0}{=} \frac{\sigma^2 r_0^2}{64\alpha_H(z_{\rm b})^{1/H}}\Big[\int dz\rho(z)\Big]\Big[\frac{4\pi\Gamma(1/H)}{H}\exp\big(-r_0^2|\boldsymbol{q}|^2\big)\exp\Big(-\frac{|\boldsymbol{x}|^2}{r_0^2}\Big) + \Phi_H^\infty\Big(\frac{\boldsymbol{x}}{\alpha_H(z_{\rm b})^{1/(2H)}}\Big)\Big], \tag{8.24}$$

and in particular

$$W_{\rm b}(\boldsymbol{0},\varepsilon\boldsymbol{q}) \stackrel{\varepsilon\to 0}{=} \frac{\sigma^2\pi\Gamma(1/H)r_0^2}{64H\alpha_H(z_{\rm b})^{1/H}}\Big[\int dz\rho(z)\Big]\Big[1+4\exp\big(-r_0^2|\boldsymbol{q}|^2\big)\Big].$$

This shows that the width of the enhanced backscattering cone is $\varepsilon q_{\rm b}$ with

$$q_{\rm b} = \frac{1}{r_0},$$

and the enhancement factor is $A_{\rm b} = 5$.

If we consider the total energy flux density $\mathbb{E}[|\hat u(0,\varepsilon\boldsymbol{q})|^2]$, then from (8.19) we have

$$\varepsilon^2\mathbb{E}[|\hat u(0,\varepsilon\boldsymbol{q})|^2] \stackrel{\varepsilon\to 0}{=} \frac{\sigma^2\pi^2 r_0^2}{16}\Big[\int dz\rho(z)\Big]\Big[1+\frac{r_0^2}{4\pi}\Psi_H(\boldsymbol{q},z_{\rm b})\Big]. \tag{8.25}$$

The width of the cone is again the width of the function $\boldsymbol{q}\to\Psi_H(\boldsymbol{q},z_{\rm b})$ and the enhancement factor is a decreasing function of $\alpha_H(z_{\rm b})r_0^{-2H}$,

$$A_{\rm b} = 1+\frac{1}{\pi}\int\exp\big(-|\boldsymbol{u}|^2-\alpha_H(z_{\rm b})r_0^{-2H}|\boldsymbol{u}|^{2H}\big)d\boldsymbol{u}.$$

This means that $A_{\rm b}$ goes from the value 2 when $\alpha_H(z_{\rm b})r_0^{-2H}\ll 1$ to the value $1+\alpha_H(z_{\rm b})^{-1/(2H)}r_0^2\Gamma(1/H)/H$, that goes to 1, when $\alpha_H(z_{\rm b})r_0^{-2H}\gg 1$.

9. Numerical Simulations. In this section we give results of numerical simulations to illustrate the theoretical results. The numerical simulations are performed in the paraxial regime with a smooth strongly scattering random medium in a one-dimensional transverse space, instead of two-dimensional transverse space as assumed in the theoretical sections of the paper. As a consequence the theoretical formulas are modified. In particular, the total energy flux density $\mathbb{E}[|\hat u(0,\varepsilon q)|^2]$ has the form

$$\varepsilon^2\mathbb{E}[|\hat u(0,\varepsilon q)|^2] \stackrel{\varepsilon\to 0}{=} \frac{\pi\sigma^2 r_0}{16}\Big[\int dz\rho(z)\Big]\Big[1+\frac{r_0}{\sqrt{r_0^2+\frac{\gamma z_{\rm b}^3}{12}}}\exp\Big(-\frac{|q|^2 r_0^2\frac{\gamma z_{\rm b}^3}{12}}{r_0^2+\frac{\gamma z_{\rm b}^3}{12}}\Big)\Big], \tag{9.1}$$

instead of (8.10), where we assume that the covariance function can be expanded as $C(x) = C(0)-\gamma x^2/2+o(x^2)$.

We assume a Gaussian input beam with carrier wavenumber $k_0 = 1$ and radius $r_0 = 64$. The Poisson cloud is at the distance $z_{\rm b} = 400$ with a thickness equal to 5. The random medium is modeled by a Gaussian process with Gaussian autocorrelation function $C(x) = \sigma_c^2\exp(-x^2/l_c^2)$ with transverse correlation radius $l_c = 4$, 8, or 16, and standard deviation $\sigma_c = 0.2$. Here $k_0^2C(0)z_{\rm b}/2 = 8$, so we are indeed in the strongly scattering regime. For $l_c = 4$, we have $\gamma = 5\,10^{-3}$, for $l_c = 8$ we have

$\gamma = 1.25\,10^{-3}$ and for $l_c = 16$ we have $\gamma = 3.125\,10^{-4}$. We use a split-step Fourier method for discretizing the paraxial wave propagation. Finally, we perform a series of 20000 independent simulations (with independent realizations of the random medium and of the Poisson cloud of scatterers) to compute the empirical average of the total energy flux density $I(q) = |\hat{u}(0,q)|^2$. Then we compare in Figure 9.1 the empirical average with with the theoretical formula (9.1) for the statistical average, which gives very good agreement. Note, however, that it is necessary to average over a lot of realizations to get the average values.

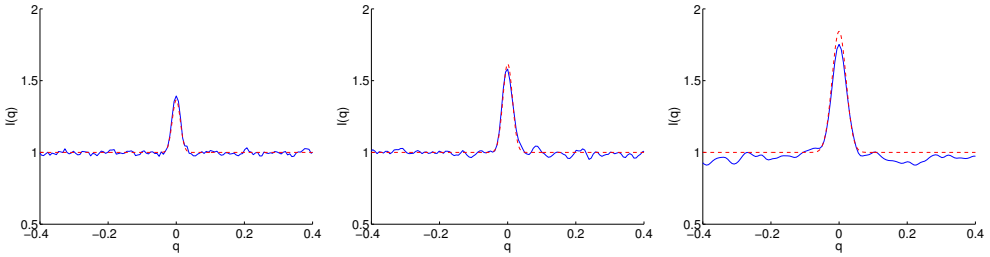

FIG. 9.1. *Mean energy flux density profiles $I(q) = |\hat{u}(0,q)|^2$ of the backscattered wave. The blue solid lines are the results of the numerical simulations. The red dashed lines are the theoretical formulas (9.1). $l_c = 4$ (left), $l_c = 8$ (center), and $l_c = 16$ (right).*

10. Conclusion. In this paper we have characterized the multiscale behavior of the Wigner distribution of the waves backscattered from a cloud of point scatterers and propagating through a turbulent medium (Proposition 7.2). This has allowed us to describe quantitatively the enhanced backscattering phenomenon. We have shown that it is possible to estimate the statistical properties of the turbulent medium from the wave backscattering in the scintillation regime. This requires to look at the angular distribution of the received backscattered wave energy flux, and not at the spatial distribution of the wave intensity. In practice, it is possible to use the time-windowing technique in order to select the contributions of the waves backscattered from a given distance z_b from an extended Poisson cloud of point scatterers. By doing so, and by fitting the measured Wigner transform, that is to say, the angular distribution of the received wave energy flux, it is possible to estimate both the Hurst parameter H and the medium parameter γ_H from the shape of the enhanced backscattering cone. This could be useful for instance to implement efficient deblurring strategies in imaging through the atmosphere [23, 28].
Note that the Wigner transform or the angular distribution of the backscattered energy flux are not statistically stable quantities. This means that it is necessary to average over many shots to ensure the statistical stability of the measured quantities and allow for their processing for medium parameter estimation.

Acknowledgements. This work was partly supported by AFOSR grant # FA9550-11-1-0176 and by ERC Advanced Grant Project MULTIMOD-267184.

Appendix A. Proof of Proposition 7.1. Here we give a detailed proof of Proposition 7.1. We denote by $\|\cdot\|_\infty$ the $L^\infty(\mathbb{R}^2 \times \mathbb{R}^2)$-norm:

$$\|M\|_\infty = \sup_{\boldsymbol{\xi},\boldsymbol{\zeta} \in \mathbb{R}^2} |M(\boldsymbol{\xi},\boldsymbol{\zeta})|.$$

For any $z \geq 0$ we introduce the linear operator $\mathcal{F}_z^\varepsilon$ that is bounded from $L^\infty(\mathbb{R}^2 \times \mathbb{R}^2)$ to $L^\infty(\mathbb{R}^2 \times \mathbb{R}^2)$ with a norm smaller than $2k_0^2 C(\mathbf{0})$:

$$\begin{aligned}\mathcal{F}_z^\varepsilon M(\boldsymbol{\xi},\boldsymbol{\zeta}) = \frac{k_0^2}{4(2\pi)^2}\int \hat{C}(\boldsymbol{k})\Big[&2M(\boldsymbol{\xi}-\boldsymbol{k},\boldsymbol{\zeta})e^{i\frac{z}{\varepsilon k_0}\boldsymbol{k}\cdot\boldsymbol{\zeta}} + 2M(\boldsymbol{\xi},\boldsymbol{\zeta}-\boldsymbol{k})e^{i\frac{z}{\varepsilon k_0}\boldsymbol{k}\cdot\boldsymbol{\xi}}\\ &-2M(\boldsymbol{\xi},\boldsymbol{\zeta}) - M(\boldsymbol{\xi}-\boldsymbol{k},\boldsymbol{\zeta}-\boldsymbol{k})e^{i\frac{z}{\varepsilon k_0}(\boldsymbol{k}\cdot(\boldsymbol{\xi}+\boldsymbol{\zeta})-|\boldsymbol{k}|^2)}\\ &-M(\boldsymbol{\xi}+\boldsymbol{k},\boldsymbol{\zeta}-\boldsymbol{k})e^{i\frac{z}{\varepsilon k_0}(\boldsymbol{k}\cdot(\boldsymbol{\xi}-\boldsymbol{\zeta})+|\boldsymbol{k}|^2)}\Big]d\boldsymbol{k}. \end{aligned} \tag{A.1}$$

We denote

$$\tilde{R}_z^\varepsilon(\boldsymbol{\xi},\boldsymbol{\zeta}) = \tilde{M}^\varepsilon(z,\boldsymbol{\xi},\boldsymbol{\zeta}) - \Big(\tilde{M}^0\big(z,\frac{\boldsymbol{\xi}}{\varepsilon}\big) + \tilde{M}^0\big(z,\frac{\boldsymbol{\zeta}}{\varepsilon}\big) - \exp\big(-\frac{k_0^2 C(\mathbf{0})z}{2}\big)\Big). \tag{A.2}$$

We need to show that $\sup_{z\in[0,Z]}\|\tilde{R}_z^\varepsilon\|_\infty$ converges to 0 as $\varepsilon \to 0$. By denoting

$$\tilde{N}_z(\boldsymbol{\xi}) = \tilde{M}^0(z,\boldsymbol{\xi}) - \exp\big(-\frac{k_0^2 C(\mathbf{0})z}{2}\big), \tag{A.3}$$

we find that $\tilde{R}_z^\varepsilon$ is solution of

$$\frac{\partial \tilde{R}_z^\varepsilon}{\partial z} = \mathcal{F}_z^\varepsilon \tilde{R}_z^\varepsilon + S_z^\varepsilon + T_z^\varepsilon,$$

starting from $\tilde{R}_{z=0}^\varepsilon(\boldsymbol{\xi},\boldsymbol{\zeta}) = 0$. Here we have introduced

$$\begin{aligned} S_z^\varepsilon(\boldsymbol{\xi},\boldsymbol{\zeta}) = &\frac{k_0^2}{2(2\pi)^2}\int \hat{C}(\boldsymbol{k})e^{i\frac{z}{\varepsilon k_0}\boldsymbol{k}\cdot\boldsymbol{\zeta}}\tilde{N}_z\big(\frac{\boldsymbol{\xi}-\boldsymbol{k}}{\varepsilon}\big)d\boldsymbol{k}\\ &+\frac{k_0^2}{2(2\pi)^2}\int \hat{C}(\boldsymbol{k})e^{i\frac{z}{\varepsilon k_0}\boldsymbol{k}\cdot\boldsymbol{\xi}}\tilde{N}_z\big(\frac{\boldsymbol{\zeta}-\boldsymbol{k}}{\varepsilon}\big)d\boldsymbol{k}\\ &-\frac{k_0^2}{4(2\pi)^2}\int \hat{C}(\boldsymbol{k})e^{i\frac{z}{\varepsilon k_0}(\boldsymbol{k}\cdot(\boldsymbol{\xi}+\boldsymbol{\zeta})-|\boldsymbol{k}|^2)}\Big(\tilde{N}_z\big(\frac{\boldsymbol{\xi}-\boldsymbol{k}}{\varepsilon}\big)+\tilde{N}_z\big(\frac{\boldsymbol{\zeta}-\boldsymbol{k}}{\varepsilon}\big)\Big)d\boldsymbol{k}\\ &-\frac{k_0^2}{4(2\pi)^2}\int \hat{C}(\boldsymbol{k})e^{i\frac{z}{\varepsilon k_0}(\boldsymbol{k}\cdot(\boldsymbol{\xi}-\boldsymbol{\zeta})+|\boldsymbol{k}|^2)}\Big(\tilde{N}_z\big(\frac{\boldsymbol{\xi}+\boldsymbol{k}}{\varepsilon}\big)+\tilde{N}_z\big(\frac{\boldsymbol{\zeta}-\boldsymbol{k}}{\varepsilon}\big)\Big)d\boldsymbol{k},\\ T_z^\varepsilon(\boldsymbol{\xi},\boldsymbol{\zeta}) = &-\exp\big(-\frac{k_0^2 C(\mathbf{0})z}{2}\big)\frac{k_0^2}{4(2\pi)^2}\int \hat{C}(\boldsymbol{k})\Big(e^{i\frac{z}{\varepsilon k_0}(\boldsymbol{k}\cdot(\boldsymbol{\xi}+\boldsymbol{\zeta})-|\boldsymbol{k}|^2)}\\ &+e^{i\frac{z}{\varepsilon k_0}(\boldsymbol{k}\cdot(\boldsymbol{\xi}-\boldsymbol{\zeta})+|\boldsymbol{k}|^2)}\Big)d\boldsymbol{k}. \end{aligned}$$

Step 1. For any $\eta > 0$,

$$\sup_{z\in[0,\eta]}\|\tilde{R}_z^\varepsilon\|_\infty \leq 4k_0^2 C(\mathbf{0})\eta e^{2k_0^2 C(\mathbf{0})\eta},$$

uniformly in $\varepsilon > 0$.
Since $\tilde{N}_z$ is bounded by 1 in $L^\infty(\mathbb{R}^2)$ uniformly in z, S_z^ε and T_z^ε are bounded by $2k_0^2 C(\mathbf{0})$ in $L^\infty(\mathbb{R}^2 \times \mathbb{R}^2)$ uniformly in z. Therefore for any $z \in [0,\eta]$ we have

$$\|\tilde{R}_z^\varepsilon\|_\infty \leq 2k_0^2 C(\mathbf{0})\int_0^z \|\tilde{R}_{z'}^\varepsilon\|_\infty dz' + 4k_0^2 C(\mathbf{0})\eta$$

By Gronwall lemma we get the desired result.

Step 2. For any $Z > \eta > 0$,

$$\sup_{z\in[0,Z]} \|\tilde R_z^\varepsilon\|_\infty \le \Big[4k_0^2 C(\mathbf{0})\eta e^{2k_0^2 C(\mathbf{0})\eta} + (Z-\eta)\sup_{z\in[\eta,Z]}\big(\|S_z^\varepsilon\|_\infty + \|T_z^\varepsilon\|_\infty\big)\Big] e^{2k_0^2 C(\mathbf{0})(Z-\eta)},$$

uniformly in $\varepsilon > 0$.
For any $z \in [\eta, Z]$ we have

$$\|\tilde R_z^\varepsilon\|_\infty \le 2k_0^2 C(\mathbf{0})\int_\eta^z \|\tilde R_{z'}^\varepsilon\|_\infty dz' + \|\tilde R_\eta^\varepsilon\|_\infty + (Z-\eta)\sup_{z'\in[\eta,Z]}\big(\|S_{z'}^\varepsilon\|_\infty + \|T_{z'}^\varepsilon\|_\infty\big).$$

By Gronwall lemma we find

$$\sup_{z\in[\eta,Z]} \|\tilde R_z^\varepsilon\|_\infty \le \Big[\|\tilde R_\eta^\varepsilon\|_\infty + (Z-\eta)\sup_{z\in[\eta,Z]}\big(\|S_z^\varepsilon\|_\infty + \|T_z^\varepsilon\|_\infty\big)\Big] e^{2k_0^2 C(\mathbf{0})(Z-\eta)},$$

which completes the proof of Step 2 by using Step 1.

Step 3. For any $Z > 0$, $\sup_{z\in[0,Z]} \|S_z^\varepsilon\|_\infty$ goes to zero as $\varepsilon \to 0$.
It is sufficient to show that, for any $Z > 0$,

$$\sup_{z\in[0,Z],\boldsymbol{\xi}\in\mathbb{R}^2} \Big| \int \hat C(\boldsymbol{k})\big|\tilde N_z\big(\frac{\boldsymbol{\xi}-\boldsymbol{k}}{\varepsilon}\big)\big| d\boldsymbol{k}\Big| \overset{\varepsilon\to 0}{\longrightarrow} 0.$$

First we remark that

$$\big|\tilde N_z\big(\frac{\boldsymbol{k}}{\varepsilon}\big)\big| = \exp\big(-\frac{k_0^2 C(\mathbf{0})z}{2}\big)\Big|\exp\big(\frac{k_0^2}{2}\int_0^z C\big(\frac{z'\boldsymbol{k}}{\varepsilon k_0}\big)dz'\big) - 1\Big| \le \frac{k_0^2}{2}\int_0^z \big|C\big(\frac{z'\boldsymbol{k}}{\varepsilon k_0}\big)\big| dz',$$

because $e^x - 1 \le e^x x$ for any $x \ge 0$ and $\sup_{\boldsymbol{x}\in\mathbb{R}^2}|C(\boldsymbol{x})| \le C(\mathbf{0})$. On the one hand, we have for any $\boldsymbol{k}$

$$\big|\tilde N_z\big(\frac{\boldsymbol{k}}{\varepsilon}\big)\big| \le \frac{k_0^2}{2} C(\mathbf{0}) z,$$

and on the other hand, for any $\boldsymbol{k} \neq \mathbf{0}$,

$$\big|\tilde N_z\big(\frac{\boldsymbol{k}}{\varepsilon}\big)\big| \le \frac{\varepsilon k_0^3}{2|\boldsymbol{k}|}\int_0^{(z|\boldsymbol{k}|)/(\varepsilon k_0)} \big|C\big(\frac{s\boldsymbol{k}}{|\boldsymbol{k}|}\big)\big| ds \le \frac{\varepsilon k_0^3}{2|\boldsymbol{k}|}\int_0^\infty \big|C\big(\frac{s\boldsymbol{k}}{|\boldsymbol{k}|}\big)\big| ds,$$

which shows that, for $\boldsymbol{k} \in \mathbb{R}^2$ and any $z \in [0, Z]$:

$$\big|\tilde N_z\big(\frac{\boldsymbol{k}}{\varepsilon}\big)\big| \le K\Big(\frac{\varepsilon}{|\boldsymbol{k}|} \wedge 1\Big),$$

where the constant K depends only on Z, k_0, $C(\mathbf{0})$, and $\sup_{\hat{\boldsymbol{e}}\in\mathbb{S}^1}\int_0^\infty |C(\hat{\boldsymbol{e}}s)|ds$. This gives for any $\boldsymbol{\xi} \in \mathbb{R}^2$, $\varepsilon < 1$, and any $z \in [0, Z]$:

$$\begin{aligned}
\Big|\int \hat C(\boldsymbol{\xi}-\boldsymbol{k})\big|\tilde N_z\big(\frac{\boldsymbol{k}}{\varepsilon}\big)\big| d\boldsymbol{k}\Big| &\le K\int \hat C(\boldsymbol{\xi}-\boldsymbol{k})\Big(\frac{\varepsilon}{|\boldsymbol{k}|}\wedge 1\Big)d\boldsymbol{k} \\
&\le K\Big[\int_{|\boldsymbol{k}|\le\varepsilon^{1/3}} \hat C(\boldsymbol{\xi}-\boldsymbol{k})d\boldsymbol{k} + \int_{|\boldsymbol{k}|>\varepsilon^{1/3}} \frac{\varepsilon}{|\boldsymbol{k}|}\hat C(\boldsymbol{\xi}-\boldsymbol{k})d\boldsymbol{k}\Big] \\
&\le K\Big[\pi\varepsilon^{2/3}\sup_{\boldsymbol{k}\in\mathbb{R}^2}|\hat C(\boldsymbol{k})| + \varepsilon^{2/3}\int_{\mathbb{R}^2}\hat C(\boldsymbol{\xi}-\boldsymbol{k})d\boldsymbol{k}\Big] \\
&\le K\varepsilon^{2/3}\Big[\pi\sup_{\boldsymbol{k}\in\mathbb{R}^2}|\hat C(\boldsymbol{k})| + (2\pi)^2 C(\mathbf{0})\Big],
\end{aligned}$$

which completes the proof of Step 3.

Step 4. For any $Z > \eta > 0$, $\sup_{z\in[\eta,Z]} \|T_z^\varepsilon\|_\infty$ goes to zero as $\varepsilon \to 0$. It is sufficient to show that

$$\sup_{\boldsymbol{\xi}\in\mathbb{R}^2} \Big| \int \hat{C}(\boldsymbol{k}) e^{iN(\boldsymbol{k}\cdot\boldsymbol{\xi}+|\boldsymbol{k}|^2)} d\boldsymbol{k} \Big| \overset{N\to\infty}{\longrightarrow} 0.$$

We rewrite

$$\int \hat{C}(\boldsymbol{k}) e^{iN(\boldsymbol{k}\cdot\boldsymbol{\xi}+|\boldsymbol{k}|^2)} d\boldsymbol{k} = \int \hat{C}\big(\boldsymbol{k} - \frac{\boldsymbol{\xi}}{2}\big) e^{iN|\boldsymbol{k}|^2 - iN\frac{|\boldsymbol{\xi}|^2}{4}} d\boldsymbol{k},$$

By Parseval's formula, for any $q > 0$, we have

$$\int \hat{C}(\boldsymbol{k}) e^{iN(\boldsymbol{k}\cdot\boldsymbol{\xi}+|\boldsymbol{k}|^2) - q^2|\boldsymbol{k}|^2} d\boldsymbol{k} = \frac{\pi}{q^2 - iN} \int C(\boldsymbol{x}) e^{-\frac{|N\boldsymbol{\xi}-\boldsymbol{x}|^2}{4(q^2-iN)}} d\boldsymbol{x}.$$

Letting $q \to 0$ (and assuming $C, \hat{C} \in L^1$) gives the generalized Parseval's formula

$$\int \hat{C}(\boldsymbol{k}) e^{iN(\boldsymbol{k}\cdot\boldsymbol{\xi}+|\boldsymbol{k}|^2)} d\boldsymbol{k} = \frac{i\pi}{N} \int C(\boldsymbol{x}) e^{i\frac{\boldsymbol{\xi}}{2}\cdot\boldsymbol{x} - i\frac{|\boldsymbol{x}|^2}{4N} - iN\frac{|\boldsymbol{\xi}|^2}{4}} d\boldsymbol{x}.$$

This shows that

$$\sup_{\boldsymbol{\xi}\in\mathbb{R}^2} \Big| \int \hat{C}(\boldsymbol{k}) e^{iN(\boldsymbol{k}\cdot\boldsymbol{\xi}+|\boldsymbol{k}|^2)} d\boldsymbol{k} \Big| \le \frac{\pi}{N} \int |C(\boldsymbol{x})| d\boldsymbol{x},$$

which completes the proof of Step 4.

Step 5. For any $Z > 0$ we have

$$\lim_{\varepsilon\to 0} \sup_{z\in[0,Z]} \|\tilde{R}_z^\varepsilon\|_\infty = 0.$$

Combining Steps 2, 3 and 4, we find that, for any $Z > \eta > 0$,

$$\limsup_{\varepsilon\to 0} \sup_{z\in[0,Z]} \|\tilde{R}_z^\varepsilon\|_\infty \le 4k_0^2 C(\mathbf{0}) \eta e^{2k_0^2 C(\mathbf{0})\eta}.$$

Since this holds true for any $\eta > 0$, we can let $\eta \to 0$ to get the desired result.

REFERENCES

[1] L. C. Andrews and R. L. Philipps, *Laser Beam Propagation Through Random Media*, SPIE Press, Bellingham, 2005.

[2] G. Bal and O. Pinaud, Dynamics of wave scintillation in random media, Comm. Partial Differential Equations **35** (2010), 1176-1235.

[3] Y. N. Barabanenkov, Wave corrections for the transfer equation for backward scattering, Izv. Vyssh. Uchebn. Zaved. Radiofiz. **16** (1973), 88-96.

[4] P. Blomgren, G. Papanicolaou, and H. Zhao, Super-resolution in time-reversal acoustics, J. Acoust. Soc. Am. **111** (2002), 230-248.

[5] J. Chrzanowski, J. Kirkiewicz, and Yu. A. Kravtsov, Influence of enhanced backscattering phenomenon on laser measurements of dust and aerosols content in a turbulent atmosphere, Phys. Lett. A **300** (2002), 298-302.

[6] D. Dawson and G. Papanicolaou, A random wave process, Appl. Math. Optim. **12** (1984), 97-114.

[7] M. V. de Hoop, J. Garnier, and K. Sølna, Enhanced and specular backscattering in random media, Waves in Random and Complex Media **22** (2012), 505-530.
[8] A. C. Fannjiang, Self-averaging radiative transfer for parabolic waves, C. R. Acad. Sci. Paris, Ser. I **342** (2006), 109-114.
[9] A. Fannjiang and K. Sølna, Superresolution and duality for time-reversal of waves in random media, Phys. Lett. A **352** (2005), 22-29.
[10] R. L. Fante, Electromagnetic beam propagation in turbulent media, Proc. IEEE **63** (1975), 1669-1692.
[11] J.-P. Fouque, J. Garnier, G. Papanicolaou, and K. Sølna, *Wave Propagation and Time Reversal in Randomly Layered Media*, Springer, New York, 2007.
[12] J.-P. Fouque, G. Papanicolaou, and Y. Samuelides, Forward and Markov approximation: the strong-intensity-fluctuations regime revisited, Waves in Random Media **8** (1998), 303-314.
[13] K. Furutsu, Statistical theory of wave propagation in a random medium and the irradiance distribution function, J. Opt. Soc. Am. **62** (1972), 240-254.
[14] K. Furutsu and Y. Furuhama, Spot dancing and relative saturation phenomena of irradiance scintillation of optical beams in a random medium, Optica **20** (1973), 707-719.
[15] J. Garnier and K. Sølna, Random backscattering in the parabolic scaling, J. Stat. Phys. **131** (2008), 445-486.
[16] J. Garnier and K. Sølna, Coupled paraxial wave equations in random media in the white-noise regime, Ann. Appl. Probab. **19** (2009), 318-346.
[17] J. Garnier and K. Sølna, Scaling limits for wave pulse transmission and reflection operators, Wave Motion **46** (2009), 122-143.
[18] J. Garnier and K. Sølna, Scintillation in the white-noise paraxial regime, to appear in Comm. Partial Differential Equations.
[19] I. S. Gradshteyn and I. M. Ryzhik, *Tables of Integrals, Series, and Products*, Academic Press, San Diego, 2007.
[20] A. Ishimaru, *Wave Propagation and Scattering in Random Media*, Academic Press, San Diego, 1978.
[21] J. F. C. Kingman, *Poisson Processes*, Clarendon Press, Oxford, 1993.
[22] G. Labeyrie, F. de Tomasi, J.-C. Bernard, C. A. Müller, C. Miniatura, and R. Kaiser, Coherent backscattering of light by atoms, Phys. Rev. Lett. **83** (1999), 5266-5269.
[23] Y. Mao and J. Gilles, Non rigid geometric distortions correction - Application to atmospheric turbulence stabilization, Inverse Problems and Imaging **6** (2012), 531-546.
[24] Y. Miyahara, Stochastic evolution equations and white noise analysis, Carleton Mathematical Lecture Notes **42**, Ottawa, Canada, (1982), 1-80.
[25] G. Papanicolaou, L. Ryzhik, and K. Sølna, Self-averaging from lateral diversity in the Itô-Schrödinger equation, SIAM Multiscale Model. Simul. **6** (2007), 468-492.
[26] J. W. Strohbehn, ed., *Laser Beam Propagation in the Atmosphere*, Springer, Berlin, 1978.
[27] V. I. Tatarskii, A. Ishimaru, and V. U. Zavorotny, eds., *Wave Propagation in Random Media (Scintillation)*, SPIE Press, Bellingham, 1993.
[28] D. H. Tofsted, Reanalysis of turbulence effects on short-exposure passive imaging, Opt. Eng. **50** (2011), 016001.
[29] A. Tourin, A. Derode, P. Roux, B. A. van Tiggelen, and M. Fink, Time-dependent coherent backscattering of acoustic waves, Phys. Rev. Lett. **79** (1997), 3637-3639.
[30] B. J. Ucsinski, Analytical solution of the fourth-moment equation and interpretation as a set of phase screens, J. Opt. Soc. Am. A **2** (1985), 2077-2091.
[31] G. C. Valley and D. L. Knepp, Application of joint Gaussian statistics to interplanetary scintillation, J. Geophys. Res. **81** (1976), 4723-4730.
[32] M. P. van Albada and A. Lagendijk, Observation of weak localization of light in a random medium, Phys. Rev. Lett. **55** (1985), 2692-2695.
[33] M. C. W. van Rossum and Th. M. Nieuwenhuizen, Multiple scattering of classical waves: Microscopy, mesoscopy, and diffusion. Rev. Modern. Phys. **71** (1999), 313-371.
[34] A. M. Whitman and M. J. Beran, Two-scale solution for atmospheric scintillation, J. Opt. Soc. Am. A **2** (1985), 2133-2143.
[35] P. E. Wolf and G. Maret, Weak localization and coherent backscattering of photons in disordered media, Phys. Rev. Lett. **55** (1985), 2696-2699.
[36] I. G. Yakushkin, Moments of field propagating in randomly inhomogeneous medium in the limit of saturated fluctuations, Radiophys. Quantum Electron. **21** (1978), 835-840.